CHALMERS
UNIVERSITY OF TECHNOLOGY

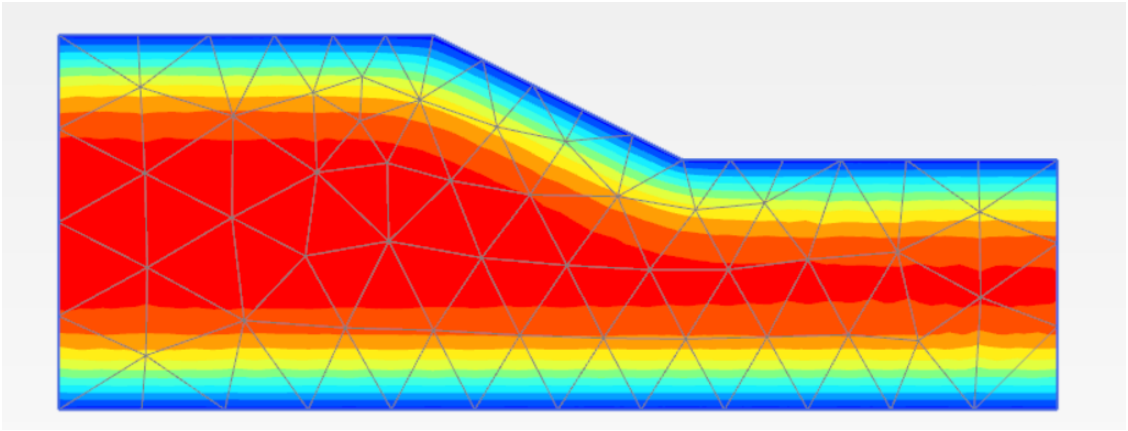

Evaluating the safety factor for slope stability under freeze-thawing cycles

Master's thesis in Master Program Infrastructure and Environmental Engineering

Jóna Björk Einarsdóttir

DEPARTMENT OF ARCHITECTURE AND CIVIL ENGINEERING

CHALMERS UNIVERSITY OF TECHNOLOGY
Gothenburg, Sweden 2024
www.chalmers.se

Master's thesis 2024

Evaluating the safety factor for slope stability under freeze-thawing cycles

Jóna Björk Einarsdóttir

CHALMERS
UNIVERSITY OF TECHNOLOGY

Department of Architecture and Civil Engineering
Division of Geology and Geotechnics
Chalmers University of Technology
Gothenburg, Sweden 2024

Evaluating the safety factor for slope stability under freeze-thawing cycles
Jóna Björk Einarsdóttir

Supervisor: Senior Lecturer Ayman Abed, Department of Architecture and Civil Engineering, Division of Geology and Geotechnics
Examiner: Senior Lecturer Ayman Abed, Department of Architecture and Civil Engineering, Division of Geology and Geotechnics

Master's Thesis 2024
Department of Architecture and Civil Engineering
Division of Geology and Geotechnics
Chalmers University of Technology
SE-412 96 Gothenburg
Telephone +46 31 772 1000

Cover: Plot of slope?

Typeset in LaTeX
Printed by Chalmers Reproservice
Gothenburg, Sweden 2024

Evaluating the safety factor for slope stability under freeze-thawing cycles
Jóna Björk Einarsdóttir
Department of Architecture and Civil Engineering
Chalmers University of Technology

Abstract

This study investigates the impact of soil freezing and thawing cycles, focusing on the climate changes in Jämtland, Sweden. A slope in this region was used as a reference to analyze slope stability during freeze-thaw cycles. PLAXIS 2D was used for slope analysis. Climate-based conditions and thermal flow in soil are the two driving factors assigned to simulate soil freezing and thawing. It was found that surface transfer is a major contributor to changes in climate conditions. After subjecting the slope to these cycles, the safety factor was calculated manually and with Python assistance. Results indicate that the slope is more stable under freezing conditions and has a higher safety factor during thawing. Although no failures were observed in the analysis, further research is recommended to incorporate freeze-thaw cycles into pre-construction planning for future urban and infrastructure development.

Keywords: Soil modelling, Freeze-Thaw cycle, Climate change, Slope stability, Safety factor.

Acknowledgements

I want to express my deepest gratitude to those who have supported and contributed to completing this thesis.

First and foremost, I am profoundly grateful to my advisor for his invaluable guidance, insightful feedback, and continuous support throughout this research. His expertise and encouragement have been instrumental in shaping this work.

I am deeply thankful to my family for their unwavering support and encouragement. Endless love and belief in me, your support has been a constant source of strength.

Thank you all for your contributions and encouragement.

Jóna Björk Einarsdóttir, Gothenburg, June 2024

List of Acronyms

Below is the list of acronyms that have been used throughout this thesis listed in alphabetical order:

BC	Boundary Conditions
BBM	Barcelona Basic Model
CPT	Cone Penetration Test
F-U	Frozen and Unfrozen soil model
NBS	Natural Based Solution
USDA	Unites States Department of Agriculture
SGI	Swedish Geotechnical Institute
SGU	Geological Survey of Sweden
SF	Safety Factor
THM	Thermo-Hydro-Mechanical

Nomenclature

Below is the vocabulary of symbols that have been used throughout this thesis.

Greek symbols

$\alpha_{x,y,z}$	Thermal expansion coefficient in x,y,z direction $[1/K]$
α	Parameter for the pressure dependency of ice thawing temperature $[-]$
β	Parameter controlling the rate of change in soil stiffness with suction $[m^2/N]$
γ	Plastic potential parameter $[-]$
γ_{water}	Unit weight of water $[N/m^3]$
κ	Elastic compressibility coefficient of the soil mixture $[-]$
κ_s	Elastic compressibility coefficient for suction variation $[-]$
κ_0	Unfrozen soil elastic compressibility coefficient $[-]$
λ	Elasto-plastic compressibility coefficient for a frozen state $[-]$
λ_0	Elasto-plastic compressibility coefficient for unfrozen state $[-]$
λ_{s1}	Thermal Conductivity $[W//(mK)]$
ν	Specific volume $[-]$
ν_f	Frozen soil Poisson's ratio $[-]$
ρ_r	Parameter for fitting unfrozen water saturation curve $[N/m^2]$
ρ_s	Density of the solid material $[kg/m^3]$

Lower case symbols

c_s	Specific heat capacity $[J/(kgK)]$
e_0	Initial void ratio $[-]$
k_t	Rate of change in apparent cohesion with suction $[-]$

m	Yield parameter $[-]$
p_{at}	Atmospheric pressure $[N/m^2]$
p_c^*	Reference stress $[N/m^2]$
p_{ref}	Parameter for the pressure dependency of ice thawing temperature $[N/m^2]$
p_{y0}^*	Pre-consolidation stress for unfrozen condition $[N/m^2]$
Δp_{y0}^*	Rate of change in p_{y0}^* with depth $[N/m^2]$
r	Coefficient related to the maximum soil stiffness $[-]$
s_c	Cryogenic suction $[N/m^2]$
$(s_{c,seg})_{in}$	Initial segregation threshold $[N/m^2]$
t	Time $[s]$

Upper case symbols

$E_{f,ref}$	Frozen Soil Young's Modulus at a reference temperature $[N/m^2]$
$E_{f,inc}$	Rate of change in Young's modulus with temperature $[N/(m^2K)]$
G	Soil shear modulus $[N/m^2]$
G_0	Soil shear modulus in unfrozen state $[N/m^2]$
K	Soil bulk modulus $[N/m^2]$
K_w	Water bulk modulus $[N/m^2]$
M	Slope of critical state line $[-]$
S_{ice}	Ice saturation
S_{sat}	Saturation in saturated conditions
S_{uw}	Unfrozen water saturation
SSA	Specific surface area $[m^2/g]$
T	Current temperature $[K]$
T_f	Freezing/melting temperature $[K]$
T_ref	Reference temperature $[K]$
Y_{ref}	Reference coordinate for $(p_{y0}^*)_in$ with deth $[m]$

Contents

List of Acronyms **ix**

Nomenclature **xi**

List of Figures **xv**

List of Tables **xix**

1 Introduction **1**
1.1 Motivation . . . 3
1.2 Aim . . . 4
1.3 Objectives . . . 4

2 Theory **5**
2.1 Impact of Climate Change on Soil . . . 5
2.1.1 Seepage and slope stability . . . 6
2.1.2 Temperature and Heat Conductivity in Soil Processes . . . 6
2.2 The Physical Characteristics of Soil in a Frozen State . . . 7
2.2.1 Cryogenic Suction . . . 7
2.2.2 Frost Heave . . . 8
2.3 Characteristics of Soil during Freezing and Thawing . . . 8
2.3.1 Thaw settlement . . . 9
2.4 Safety Factor, Ordinary method . . . 9

3 Modelling the Process of Freezing and Thawing **11**
3.1 The Constitutive Model . . . 11
3.2 Thermodynamic equilibrium . . . 12
3.3 Unfrozen Water Content . . . 13
3.4 Elastic response . . . 15
3.5 Yield surfaces . . . 17
3.6 Hardening rules . . . 17
3.7 Flow rules . . . 18
3.8 Model parameters . . . 18

4 Methods **21**
4.1 Soil properties and geometry . . . 21
4.2 Climate in the region of Jämtland . . . 23

4.3 Test model . . . 23
4.3.1 Boundary conditions . . . 23
4.3.2 Scenarios . . . 24
4.4 The Frozen and Unfrozen Model . . . 25
4.4.1 Boundary conditions . . . 25
4.5 Calculating the Safety Factor . . . 26
4.5.1 Estimating the slip surface . . . 27

5 Results **31**
5.1 Test model . . . 31
5.1.1 Heat analysis . . . 31
5.1.1.1 Scenario: Summer to Autumn . . . 31
5.1.1.2 Scenario: Winter to spring . . . 34
5.2 Frozen and unfrozen model . . . 37
5.2.1 Climate based conditions . . . 37
5.2.1.1 Temperature distribution . . . 37
5.2.1.2 Saturation analysis . . . 46
5.2.1.3 Excess pore pressure . . . 47
5.2.2 Thermal flow conditions . . . 53
5.2.2.1 Temperature distribution . . . 53
5.2.2.2 Saturation analysis . . . 56
5.2.2.3 Excess pore pressure . . . 59
5.3 Safety Factor analysis . . . 61
5.3.1 BC: Climate in Jämtland . . . 61
5.3.2 BC: Thermal flow . . . 63

6 Discussion **65**
6.1 Thermal influence . . . 65
6.2 Saturation analysis . . . 65
6.3 Excess pore pressure . . . 66
6.4 Safety factor . . . 66

7 Conclusion **67**
7.1 Limitations . . . 67
7.2 Further studies . . . 67

Bibliography **69**

A Appendix 1 **I**

B Appendix 2 **V**

C Appendix 3 **IX**

List of Figures

1.1 Changes in (a) surface temperatures and (b) precipitation from the period spanning 1986-2005 to 2081-2100.[2] 2
1.2 Location of Bispgården 3

3.1 Diagram illustrating the mechanisms of curvature-induced pre-melting and interfacial pre-melting [18] 14
3.2 Input model parameters 18

4.1 Soil Type Overview with Demonstration Trial Areas Marked in Black [12] 21
4.2 A profile of the slope 22
4.3 A profile of the slope with selected nodes. 22
4.4 Selected boundary conditions for water flow 24
4.5 Selected boundary conditions for thermal flow 24
4.6 Assigned ice saturation curve 25
4.7 Estimating the slip surface for the Bispgården slope 27
4.8 Explanations on how parameters for the SF calculations were extracted 28

5.1 Temperature distribution for the test model for summer to autumn with $1W/m^2/K$ 32
5.2 Temperature distribution for the test model for summer to autumn with $5W/m^2/K$ 33
5.3 Temperature distribution for the test model for summer to autumn with $10W/m^2/K$ 34
5.4 Temperature distribution for the test model for winter to spring with $1W/m^2/K$ 35
5.5 Temperature distribution for the test model for winter to spring with $5W/m^2/K$ 36
5.6 Temperature distribution for the test model for winter to spring with $10W/m^2/K$ 37
5.7 Profile of the temperature distribution when climate is freezing and surface transfer is $1W/m^2/K$ for (a) 20 days (b) 50 days (c) 100 days (d) 150 days 38
5.8 Temperature distribution when climate is freezing and surface transfer is $1W/m^2/K$ 38

5.9 Profile of the temperature distribution when climate is freezing and surface transfer is $5W/m^2/K$ (a) 20 days (b) 50 days (c) 100 days (d) 150 days 39
5.10 Temperature distribution when climate is freezing and surface transfer is $5W/m^2/K$ 40
5.11 Profile of the temperature distribution when climate is freezing and surface transfer is $10W/m^2/K$ (a) 20 days (b) 50 days (c) 100 days (d) 150 days 40
5.12 Temperature distribution when climate is freezing and surface transfer is $10W/m^2/K$ 41
5.13 Profile of the temperature distribution when the climate is thawing and surface transfer is $1W/m^2/K$ (a) 20 days (b) 50 days (c) 100 days (d) 150 days 42
5.14 Temperature distribution when the climate is thawing and surface transfer is $1W/m^2/K$ 42
5.15 Profile of the temperature distribution when the climate is thawing and surface transfer is $5W/m^2/K$ (a) 20 days (b) 50 days (c) 100 days (d) 150 days 43
5.16 Temperature distribution when the climate is thawing and surface transfer is $5W/m^2/K$ 44
5.17 Profile of the temperature distribution when the climate is thawing and surface transfer is $10W/m^2/K$ (a) 20 days (b) 50 days (c) 100 days (d) 150 days 45
5.18 Temperature distribution when the climate is thawing and surface transfer is $5W/m^2/K$ 45
5.19 Result on how the ice saturation is distributing over time with the different climate conditions assigned 46
5.20 Excess pore pressure when the climate is freezing and the surface transfer is $1W/m^2/K$ for (a) 20 days (b) 50 days (c) 100 days (d) 150 days 47
5.21 Excess pore pressure when the climate is freezing and the surface transfer is $5W/m^2/K$ for (a) 20 days (b) 50 days (c) 100 days (d) 150 days 49
5.22 Excess pore pressure when the climate is freezing and the surface transfer is $10W/m^2/K$ for (a) 20 days (b) 50 days (c) 100 days (d) 150 days 50
5.23 Excess pore pressure when the climate is thawing and the surface transfer is $1W/m^2/K$ for (a) 20 days (b) 50 days (c) 100 days (d) 150 days 51
5.24 Excess pore pressure when the climate is thawing and the surface transfer is $5W/m^2/K$ for (a) 20 days (b) 50 days (c) 100 days (d) 150 days 52
5.25 Excess pore pressure when the climate is thawing and the surface transfer is $10W/m^2/K$ for (a) 20 days (b) 50 days (c) 100 days (d) 150 days 53

5.26 Profile of the temperature distribution when the thermal flow is thawing in the soil for (a) 20 days (b) 50 days (c) 100 days (d) 150 days . 54
5.27 Temperature distribution when thermal flow is thawing. 54
5.28 Profile of the temperature distribution when the thermal flow is freezing in the soil for (a) 20 days (b) 50 days (c) 100 days (d) 150 days . 55
5.29 Temperature distribution when the thermal flow is freezing. 56
5.30 Profile of the ice saturation when the thermal flow is freezing in the soil for (a) 20 days (b) 50 days (c) 100 days (d) 150 days 56
5.31 Ice saturation when boundary conditions are thermal flow is freezing. 57
5.32 Profile of the ice saturation when the thermal flow is thawing in the soil for (a) 20 days (b) 50 days (c) 100 days (d) 150 days 58
5.33 Ice saturation when boundary conditions are thermal flow is thawing. 58
5.34 Profile of the excess pore pressure when the thermal flow is thawing in the soil for (a) 20 days (b) 50 days (c) 100 days (d) 150 days . . . 59
5.35 Profile of the excess pore pressure when the thermal flow is freezing in the soil for (a) 20 days (b) 50 days (c) 100 days (d) 150 days . . . 60
5.36 A distribution on how the SF is acting with different climate conditions from hand calculations 61
5.37 A distribution on how the SF is acting with different climate conditions from python code 62
5.38 A diagram illustrating the slip surface under climate conditions, with a surface transfer rate of $10w/m^2/k$ after 150 days of freezing temperature 62
5.39 A distribution on how the SF is acting with different climate conditions from hand calculations and python code 63
5.40 A diagram illustrating the slip surface under thermal flow conditions after 150 days of freezing temperature 64

List of Tables

3.1 Coefficient and exponents for freezing/melting point pressure dependency equation 13
3.2 USDA classification limits for particle size 15
3.3 Default values of elastic parameters 19

A.1 General, Mechanical, Groundwater, Thermal, Initial I
A.2 Model parameters: Water and ice I
A.3 Soil properties: General, Groundwater, Thermal and Initial II
A.4 Froze/unfrozen material properties for freezing-thawing cycle III

B.1 Temperature function: Climate conditions - Winter to spring V
B.2 Temperature function: Climate conditions - Autumn to Winter VI
B.3 Temperature function: Thermal flow - thawing VI
B.4 Temperature function: Thermal flow - freezing VII

C.1 SF calculations using hand calculations - Climate conditions IX
C.2 SF calculations using python - Climate conditions X
C.3 SF calculations hand calculations - Thermal flow XI
C.4 SF calculations using python - Thermal flow XI

1
Introduction

Geotechnical structures such as slopes are continually affected by climate-driven environmental changes. Over the past century, rapid population growth has fueled urban expansion, leading to extensive infrastructure and transportation development while intruding on natural and agricultural lands. Consequently, energy demands, environmental degradation, and associated climate changes are growing urgent concerns [1] [2].

Recent assessments by the United Nations Intergovernmental Panel on Climate Change (IPCC) highlight the extreme weather and climate conditions observed worldwide, including heatwaves, heavy precipitation, droughts, sea-level rise, and glacier melting [2]. Anthropogenic factors, including the accelerated combustion of fossil fuels, increased use of petrochemicals, and rapid changes in land use attributed to deforestation and industrialization, have significantly contributed to the worsening of climate change. This human-induced climate change, characterized by excessive greenhouse gas emissions such as carbon dioxide, methane, and nitrous oxide, has led to global warming and poses a significant threat to the well-being and survival of all living beings on Earth [15]. Additionally, in cold regions, seasonal temperature variations can lead to soil freezing near the ground surface, often accompanied by frost heave and ice segregation [10].

Considering the ongoing reality of climate change, it should be wise to integrate it into the evaluation and planning of geo-structures. Assessing climate change is vital to minimize potential devastating consequences, like damage or collapse, especially in situations where incidents such as landslides have already occurred on slopes. Looking ahead, embracing sustainable approaches becomes essential, taking into account both climate change and sustainability factors. Acting now is becoming pivotal in shaping a future where the environment and quality of life are preserved [1]. Examining the freeze-thaw cycle can help to assess the impact of certain activities on soil. The soil becomes denser when temperatures drop below zero, increasing shear strength. However, during the thawing process, excess pore pressure builds up, which reduces shear strength and could lead to slope failure, such as foundation failures [2]

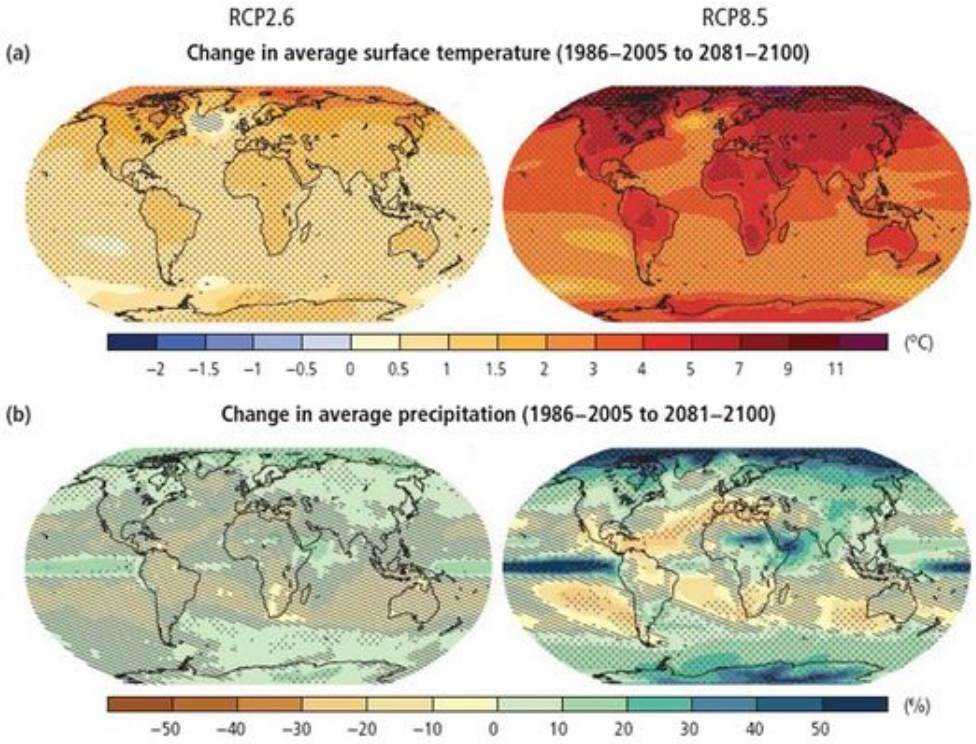

Figure 1.1: Changes in (a) surface temperatures and (b) precipitation from the period spanning 1986-2005 to 2081-2100.[2]

Other researchers have also emphasized this phenomenon's critical nature and contributed to enhancing the understanding of soil behaviour under these conditions. According to Tamara et al. (2022), the rise in net water infiltration is a key determinant of slope stability. Hence, assessing all slopes in light of projected climate change is advisable, considering its potential implications[1]. In 2015, Vardon investigated the possible impacts of climate change on geotechnical infrastructures. He emphasized the importance of predicted climate changes, including temperature, precipitation, wind, sea level rise, storms, river flow, and cold, for geotechnical infrastructure [21].

Case study

In 2002, the Swedish Geotechnical Institute (SGI) initiated a series of demonstration trials involving various types of Natural Based Solutions (NBS) in Bispgården, located in the Jämtland region of Sweden, see figure 1.2. These trials were documented in the report "*Växter som skydd mot erosion och ytliga ras i branta jordsluänter Demonstrationsförsök i Bispgården och Bydalen*" by Lundström and Andersson (2008), and serves as a reference project for this thesis. The trials were conducted in two main locations: smaller NBS types were tested along roadsides in the Bydalen area, west of Östersund, although these tests had limited geotechnical data available. Meanwhile, the Bispgården test site featured a cut slope of approximately 30° composed of silty soil, where various NBS types were tested. Unfortunately,

Figure 1.2: Location of Bispgården

the project faced premature termination when the two slope sections experienced failure in the spring of 2006. Notably, this was not the first structural issue with the slope sections. In contrast, in the previous spring, frost-and-thaw processes impacted some slope sections resulting in the breakage of roots and branches integral to the NBS and a blockage of installed drainage pipes with soil.

1.1 Motivation

These findings highlight the escalating occurrence of freeze-thaw cycles in Sweden and globally, particularly amidst rapid climate changes observed in recent decades. This emphasizes the critical importance of analyzing slope stability under such conditions. With climate change accelerating, freeze-thaw cycles are expected to become more frequent and extreme, posing significant risks to infrastructure and natural slopes. Understanding their impact on slope stability is essential for mitigating hazards like landslides and erosion. With this knowledge and the enhanced understanding of these conditions, a new evolution may arise in the approach to slope management strategies, aiming to increase resilience against climate-related uncertainties.

Exploring the impact of freezing and thawing on slope stability, particularly in regions such as the Nordic countries, requires an in-depth understanding of the underlying physical processes. This investigation aims to uncover the underlying processes and the behaviour of water in reaction to temperature changes. Significantly, there's a recognized deficiency in methods for estimating the safety factor of slopes in such conditions, prompting the need for further study. A thorough literature review could potentially reveal past approaches and gaps in knowledge, thereby motivating the current research endeavour. In geotechnical design practices, long-term stability assessments of soil slopes, such as embankment slopes and cut slopes along highways, often overlook factors like freeze-thaw action and snow melt water infiltration [22].

1.2 Aim

The study aims to investigate the impact of soil freezing and thawing, driven by rapid climate change, on slope stability models. This investigation will address the following research questions:

1. How does the process of freezing and thawing contribute to slope stability hazards?
2. Could advanced coupled Thermo-Hydro-Mechanical (THM) Finite Element (FE) analysis effectively model and predict these processes?
3. How do the findings contribute to a deeper understanding of the factors influencing slope stability and the safety factor of the slope under freeze-thaw conditions?

1.3 Objectives

The first research question will be addressed primarily through a literature review, clarifying the potential freeze thaw impacts on various types of soil within the Theory chapter. This may also include field investigations over a period of time to observe variations or laboratory experiments with soil samples undergoing controlled freeze-thaw cycles. The comprehensiveness of this understanding may be influenced by the depth and breadth of available literature.

The second and third research questions will be explored using a 2D model in a program called PLAXIS 2D. Additionally, evaluating the safety factor under these conditions will require a thorough understanding of how to calculate the safety factor effectively.

2

Theory

A slope is characterized as a surface where one end or side is positioned at a higher elevation than another, creating a rising or falling surface. An earth slope specifically refers to an unsupported, inclined surface formed by a mass of soil. When this mass of soil situated beneath a slope collapses, it is termed a slide. This event entails the downward and outward movement of the entire soil mass involved in the failure. Essentially, a slide occurs when the soil loses its stability and moves downward and outward due to gravitational forces.

Slope stability analysis is a crucial process to ensure the safety of both natural and man-made slopes. The failure of a slope can have severe consequences, including loss of life and property damage, making it imperative to examine thoroughly and understand slope stability before any construction. Advances in soil testing techniques and stability analysis methodologies have greatly enhanced the ability to design slopes that are not only safe but also economically viable. Geotechnical engineers, responsible for evaluating and designing slopes, must understand various analytical methods and their limitations to make informed decisions during the design process.

2.1 Impact of Climate Change on Soil

Identifying the cause of climate change is undeniably crucial from an environmental perspective; however, climate science often grapples with uncertainty [1]. Engineered and natural slopes face threats from climate variability, which refers to changes in weather patterns over time. These variations can result in an increase in the frequency and intensity of extreme weather events. Such alternatives are intense rainfall or extended drought periods. For slopes, these extreme weather events pose significant risks. For instance, heavy rainfall can saturate the soil, reducing its stability and increasing the likelihood of landslides. On the other hand, prolonged droughts can dry out the soil, making it more prone to erosion and slope failure [1]. In cold regions, soil near the surface may freeze, leading to frost heave and ice segregation. These processes cause engineering issues such as pavement cracking, foundation damage, and pipeline fractures [10].

2.1.1 Seepage and slope stability

Seepage stands out as a critical factor influencing stability, with many landslides attributed to its effects. It denotes the movement of water through the soil under the influence of gravity and hydraulic forces. Initially, water arrives on the slope surface via precipitation, where a portion is intercepted and evaporated by foliage and branches—an occurrence known as interception. Once this interception is depleted, the remaining precipitation water reaches the soil surface. Some of it flows over the ground as overland runoff when precipitation exceeds the soil's infiltration capacity, while the rest infiltrates into the soil [**?**].

The infiltration of rainwater into a hill slope alters its water content, pore pressure, and groundwater table. This has a significant impact on slope stability, as it modifies factors such as total unit weight, effective stress, suction stress, and matric suction across the hill slope [1]

The occurrence of overland runoff on a slope hinges on several factors, including the slope angle, vegetation cover, and surface roughness. Meanwhile, the rate of infiltration is primarily governed by the soil's hydraulic conductivity, which fluctuates with changes in soil suction [1].

2.1.2 Temperature and Heat Conductivity in Soil Processes

Temperature significantly impacts numerous processes within soils. Among these, are frost heaving, weathering, and organic matter. Decomposition is a notable example of physical and chemical processes influenced by temperature. Soil temperatures result from heat transport processes within the soil and heat exchange between the soil and the atmosphere. At the soil surface, thermal exchange processes are primarily dictated by meteorological conditions and occur through radiation, conduction, and convection. Furthermore, the thermal properties of soil are greatly influenced by its water content [3].

Soil heat conductivity, λ, refers to how effectively heat flows through the soil. It is calculated as the heat flux density, or the amount of heat passing through a unit area of soil per unit of time, divided by the temperature gradient, which is the change in temperature over a given distance. The value of soil heat conductivity is heavily influenced by how highly conductive mineral particles are connected by the less conductive water phase and separated by the poorly conductive gas phase. Essentially, the more connected the mineral particles are, the better the soil conducts heat. Soil air has minimal impact on heat conductivity because the air itself has a very low heat conductivity. When dry soil gains a small amount of water, there is only a slight increase in heat conductivity. This is because the water forms thin films around soil particles rather than filling the pore spaces. The highest level of heat conductivity occurs when the soil is fully saturated with water. At this point, the soil conducts heat most efficiently [3].

2.2 The Physical Characteristics of Soil in a Frozen State

Cold climates experience seasonal temperature changes that lead to the freezing of soil near the ground surface. The freezing point in soil marks the temperature at which water transitions from a liquid to a solid state (ice) under normal atmospheric pressure, typically around 0°C (273.15 K) for pure water. As surface temperatures drop below this point, soil moisture begins to freeze, forming ice crystals and potentially expanding soil particles. The process of soil freezing is complex and involves multiple interacting factors, including heat transfer, moisture transfer, and force equilibrium. Pore water within the soil undergoes phase changes during this process, further complicating the phenomenon [10].

Moreover, as the surface temperature of a soil sample falls below the freezing point, the freezing front advances into the sample. The freezing front defines the boundary between frozen and unfrozen soil, progressively penetrating deeper into the soil as temperatures decrease. This progression occurs as heat is extracted from the soil, causing moisture within it to freeze and expand, driving the advancement of the freezing front downward into the soil mass.

Frozen soils often contain significant water that has not yet frozen. When there are differences in water pressure within the soil due to varying hydraulic gradients, this unfrozen water can move. This movement of water within frozen soil plays a crucial role in a phenomenon known as frost heave. Additionally, the stability of slopes can be influenced by the movement of water within frozen soils (Burt & Williams, 1976).

The type of soil is a crucial factor in determining how water can move through frozen soil. This is primarily because the presence of unfrozen water is dependent on factors such as pore size distribution, void ratio, particle size, and surface area. These characteristics of the soil influence its hydraulic conductivity when frozen(Burt & Williams, 1976).

According to Nishimura et al. (2009) when water freezes within the soil, it expands by approximately 9% resulting in a volumetric strain in the soil. The expansion occurs because water molecules arrange themselves into a crystalline structure when freezing, causing an increase in volume. The degree of volumetric strain depends on various factors, including the soil porosity, which influences how much water is presented to freeze and expand [8].

2.2.1 Cryogenic Suction

When the soil temperature drops below the freezing point, a phase change of pore water occurs within the frozen fringe. The frozen fringe refers to the region within the soil where freezing occurs. This is typically at the boundary between the frozen and unfrozen portions of the soil. When water freezes, it expands in volume. This

expansion leads to an increase in pressure within the unfrozen pores of the soil. As the temperature decreases towards the freezing front, there's a gradient in suction force created. This force, known as cryogenic suction, draws the unfrozen pore water towards the freezing front. The movement of unfrozen water towards the freezing front increases the pressure within the pores in that region. This elevation of pore pressure contributes to various soil processes and phenomena, such as frost heave and ice segregation [10].

2.2.2 Frost Heave

Frost heave, which refers to the upward movement of soil or other surface material caused by water freezing within the soil, is commonly explained by the volume change that occurs during water freezing. This expansion occurs upward due to less resistance in that direction (Taber, 1929). Specifically, the movement of water within soil plays a significant role in causing frost heaving, leading to a decrease in bearing capacity after thawing (Fremond, 1982).

Frost heave is characterized not only by the movement of liquid water but also by the formation of distinct patterns within the soil. It tends to create bands of ice lenses absent of particles, separated by layers of soil infiltrated by ice. These ice lenses are essentially layers of pure ice that develop within the soil. Between these ice lenses, there are layers of soil that contain a mixture of soil particles and ice. This pattern results from the movement of water within the soil as it freezes, with water migrating to the freezing front and forming these ice lenses, while the soil between them remains partially frozen with ice mixed into it (Rempel, 2010).

2.3 Characteristics of Soil during Freezing and Thawing

The expansion and contraction of soil due to freezing and thawing cycles have caused damage to infrastructure such as roads, foundations and agricultural activities (Taber, 1929). As mentioned earlier, freezing and thawing cycles are common in regions with cold climates. The transition between frozen and unfrozen soil, known as a phase change, is governed by the Clausius-Clapeyron equation (Equation 3.2) [**?**].

During the freezing phase, soil acts as a solid porous material with significantly higher strength. Studies show that at low confining pressures, the strength of frozen soil increases with pressure. However, beyond a certain threshold, additional pressure decreases strength before increasing it again. This complex behaviour arises from mechanical effects, affecting stress distribution, and thermodynamic effects, involving pressure melting. Pressure melting lowers the ice-thawing temperature, reducing cryogenic suction and increasing water pressure. [**?**]

During the thaw phase of the freeze-thaw cycle, periglacial solifluction occurs, partic-

ularly on slopes. This refers to the slow movement of soil or sediment downslope due to water within the soil layers [10]. The Clausius-Clapeyron equation, derived from the equilibrium of chemical potentials between two phases, describes the equilibrium between liquid water and ice phases. See Equation 3.2 on how this is expressed.

The ice forms a solid structure where a water film develops around soil grains, leading to water-filled pores. The effective stress in this material is referred to as solid phase stress and is considered the combined stress of soil grains and ice. Solid phase stress is defined by Equation 3.1 (Aukenthaler, 2015).

2.3.1 Thaw settlement

Upon thawing, the ice within the soil melts, prompting the soil structure to adjust to a new equilibrium void ratio under existing overburden pressures. This adjustment triggers volume changes in the soil, resulting from both the phase change of ice to water and the drainage of excess water from the soil. Soils with higher ice content, such as silts and clayey silts, typically experience more significant thaw settlements. When frozen soil experiences a temperature increase, the thawing process is influenced by temperature boundary conditions and soil thermal properties. Thawing slowly allows water generated from melting to flow out of the soil gradually, matching the melting rate. Consequently, excess pore pressures are not sustained, and settlement progresses concurrently with thawing. However, faster thawing rates lead to the generation of excess pore pressures within the soil. These excess pressures diminish the soil's shear strength, potentially resulting in unstable conditions for foundations or slopes [9].

2.4 Safety Factor, Ordinary method

The Ordinary Method of Slices, credited to Fellenius in 1927, is a fundamental technique in slope stability analysis. It involves breaking down the mass of soil above the potential failure surface into discrete slices, allowing engineers to analyse each slice individually. The method aims to determine whether the slope is stable or prone to failure by considering the equilibrium of forces and moments acting on each slice. A key assumption of this method is that the resultant forces on each slice act parallel to its base, simplifying the analysis. However, it's important to note that this approach doesn't fully satisfy Newton's third law, as the forces on adjacent slices may not perfectly balance each other. Despite this limitation, the method remains widely used due to its simplicity and effectiveness in evaluating slope stability [16].

In the method of slice analysis, only one equation is employed to ensure the moment of equilibrium across the entire mass of the soil. Consequently, the calculation yields only one unknown: the factor of safety. This simplicity in determining the factor of safety is a key characteristic of this method [16].

The analysis assumes that the slope under consideration extends infinitely in both horizontal directions. This simplifying assumption aids in mathematical modelling but may not accurately represent real-world conditions. The method assumes that the slip surface, along which the failure occurs, is parallel to the ground surface. This simplifies the analysis but may not capture the complexities of actual slope failures where the slip surface may not align perfectly with the ground surface. The method neglects the interaction forces between adjacent slices of the slope. This simplification may lead to inaccuracies, especially in situations where such interactions play a significant role [16].

It is most applicable to homogeneous slopes and soils with known cohesion (c) and angle of internal friction (ϕ). It may yield satisfactory results for these conditions, particularly when the circular slip surface assumption holds. The method is convenient for performing manual calculations due to its simplicity, making it suitable for quick assessments or preliminary analyses. In situations where accurate assessments of effective stress under high pore pressures are required, this method may not provide reliable results. Its neglect of inter-slice forces and assumptions about slip surface orientation can lead to inaccuracies in effective stress analyses [16].

The assumptions listed are fundamental simplifications made in the analysis of slope stability using this method. While these assumptions facilitate mathematical modelling and hand calculations, they may not accurately represent real-world slope conditions. The limitations and applications outlined provide insights into when and where this method is appropriate and when caution should be exercised. Overall, understanding the assumptions, limitations, and applications of the method is crucial for its effective use in slope stability analysis [16].

3

Modelling the Process of Freezing and Thawing

The computational methods employed to assess each component of the water balance are intricate and rely on numerous assumptions. Finite element software analysis offers a means to examine slope stability and the behaviour of water infiltration under precipitation conditions. Factors influencing soil, such as internal friction angle, water content, hydraulic conductivity, as well as the duration and intensity of precipitation, are integral parts of the analysis [1].

Studying the behaviour of frozen soils with THM coupling typically necessitates a numerical approach like the finite element method (FEM) due to the nonlinear nature of the governing equations and their mutual interaction [8].

The freezing and thawing of pore fluid in soils entail intricate thermal, hydraulic, and mechanical processes with substantial mutual geotechnical interactions. These processes interact, meaning changes in one process can affect the others. For example, when the temperature changes cause the pore fluid to freeze or thaw, it affects the hydraulic behaviour of the soil, which then influences its mechanical deformation. These interconnections demonstrate the complex nature of soil behaviour during freezing and thawing processes [8].

3.1 The Constitutive Model

The elastic-plastic frozen/unfrozen soil model, developed by Amiri, Grimstad, Kadivar, & Nordal (2016) and later modified by Aukenthaler (2016) for Plaxis, simulates the mechanical behaviour of frozen soil under various loads and predicts deformation during freezing and thawing. It uses two stress state variables: solid phase stress and cryogenic suction. The solid phase stress, defined by Equation 3.1, represents the combined stress in soil grains and ice, with I denoting the unit tensor (compression is negative) [17].

$$\sigma* = \sigma - S_{uw} P_w I \tag{3.1}$$

As well as σ^* is the solid phase stress tensor, σ is the total stress tensor, S_w is the unfrozen water saturation and P_w is the pore water pressure [17]. The elastic-plastic features in the model effectively replicate the probable behaviour of the soil skeleton

during loosening and segregation [8].

In this model, saturated frozen soil is treated as a porous material of soil grains and ice, with water filling the pores. Ice is included in the solid phase stress because it can bear shear stresses. This formulation uses a Bishop-type effective stress approach, where the unfrozen water saturation S_{uw} acts as the effective stress parameter, also known as the Bishop parameter. The solid phase stress accounts for the influence of unfrozen water on the soil's mechanical behaviour. Cryogenic suction is the second state variable in the model, allowing for a comprehensive hydro-mechanical framework. By incorporating cryogenic suction, the model can account for the effects of ice content and temperature variations [17].

3.2 Thermodynamic equilibrium

The Clausius-Clapeyron equation, equation 3.2, is a fundamental concept in thermodynamics, that allows us to pinpoint the forces driving pore water flow due to temperature variations. This equation provides insights into how temperature discrepancies prompt water movement through porous materials by detailing the interplay among pressure, temperature, and volume during phase transitions. It clarifies the thermally driven mechanisms guiding pore water flow [10]

$$\frac{p_{ice}}{\rho_{ice}} - \frac{p_w}{\rho_w} = L \ln(\frac{T}{T_f}) \tag{3.2}$$

In the given scenario, p_{ice} and p_w denote the pressures of ice and pore water respectively. Similarly, ρ_{ice} and ρ_w represent ice and pore water densities. The symbol L corresponds to the latent heat of fusion, while T stands for the current temperature, and T_f signifies the freezing or melting temperature under the prevailing pressure conditions [17].

Utilizing the Clausius-Clapeyron equation, the equation for cryogenic suction, equation 3.5, as the pressure difference between pore ice and pore water can be derived:

$$s_c = p_{ice} - p_w \tag{3.3}$$

$$s_c = \rho_{ice}(\frac{p_w}{\rho_w} - L \ln(\frac{T}{T_f})) - p_w \tag{3.4}$$

If we assume that the densities of ice and water are similar, the equation simplifies to:

$$s_c \approx -\rho_{ice} L \ln(\frac{T}{T_f}) \tag{3.5}$$

The freezing point of water varies with the surrounding pressure. As the pressure increases, the freezing (or melting) temperature of water decreases, and conversely,

it increases when the pressure decreases. To estimate the freezing/thawing temperature T_f, two methods are introduced. In the method proposed by Amiri, Grimstad, Kadivar, & Nordal (2016), the freezing/thawing temperature at a given ice pressure is calculated using Equation 3.6. This equation incorporates two constant parameters [17]: p_{ref} and α, where typically $7 < \alpha < 9$, $p_{ref} = -395$ MPa, and $T_{ref} = 273.16$ K [17].

$$T_f = T_{ref}(\frac{p_{ice}}{-p_{ref}} + 1)^{\frac{1}{\alpha}} \tag{3.6}$$

In this approach, the unfrozen water saturation S_{uw} in Plaxis is calculated using Equation 3.7, where ρ_r and λ_r are two constants.

$$S_{uw} = [1 + (\frac{s_c}{\rho_r})^{\frac{1}{1-\lambda_r}}]^{-}\lambda_r \tag{3.7}$$

Aukenthaler, Brinkgreve & Haxaire (2016) developed an alternative formulation. The pressure dependence of the melting temperature for ice is expressed according to Wagner, Riethmann, Feistel & Harvey (2011) by Equation 3.8. In this equation, T_t is 273.16 K and p_t is -611.657 Pa. The coefficient a_i and exponents b_i are provided in Table 3.1 [17].

$$\frac{p_{melt}}{p_t} = 1 + \sum_{1}^{3} a_i[1 - (\frac{T}{T_t}^{b_i}] \tag{3.8}$$

Which can be simplified into, Equation 3.9:

$$\frac{s_c + p_w}{611.657Pa} = 1 + \sum_{1}^{3} a_i[1 - (\frac{T}{273.16}^{b_i}] \tag{3.9}$$

i	a_i	b_i
1	$0.119539337 * 10^7$	$0.300000 * 10$
2	$0.808183159 * 10^5$	$0.257500 * 10^2$
3	$0.333826860 * 10^4$	0.103750

Table 3.1: Coefficient and exponents for freezing/melting point pressure dependency equation

3.3 Unfrozen Water Content

As previously mentioned, studying the effect of cryogenic suction is crucial for understanding the behaviour of frozen soils. Two mechanisms allow water to remain unfrozen at temperatures below the bulk freezing point: curvature-induced premelting and interfacial pre-melting see Figure 3.1

.

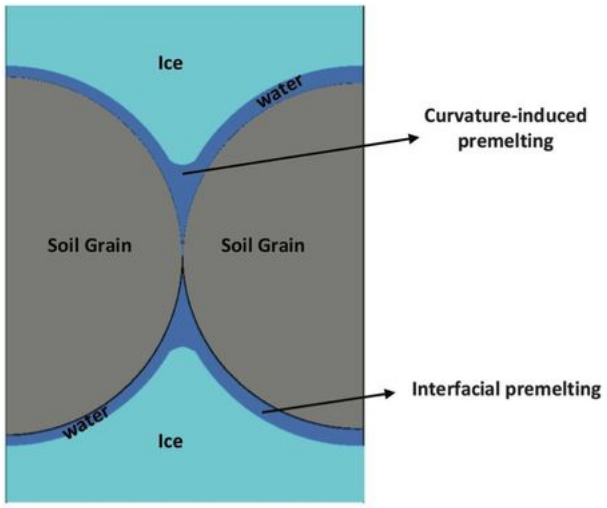

Figure 3.1: Diagram illustrating the mechanisms of curvature-induced pre-melting and interfacial pre-melting [18]

Curvature-induced pre-melting is caused by surface tension and is similar to capillary suction, bonding the soil grains together. Interfacial pre-melting, on the other hand, results from disjoining pressure, which acts as a repelling force between ice and solid grains, widening the gaps and drawing in more water. The interplay of these mechanisms determines the soil's behaviour in response to changes in ice content and temperature [**?**].

To calculate the remaining unfrozen water in the soil relative to temperature, two approaches are outlined in the model manual by Ghoreishian Amiri et al. (2016). The unfrozen water saturation, S_{uw}, can be calculated and fitted to experimental results using a formulation based on the van Genuchten model (van Genuchten, 1980) as proposed by Nishimura et al. (2009), shown in Equation 3.7 [17].

The unfrozen water content is related to the volumetric unfrozen water content. This relationship, in turn, is connected to the temperature through an empirical formulation based on the findings of Anderson & Tice (1972). Equation (2.24) provides this empirical relationship, which is only valid for $T \leq T_{f,bulk}$ (ref: the manual). Equation 3.10 calculates the volumetric unfrozen water content, θ_{uw}. It considers the soil-specific surface area (SSA), the bulk density of soil (ρ_b), and its temperature (T & $T_{f,bulk}$) as inputs.

$$\theta_{uw} = \frac{\rho_w}{\rho_b} exp(0.2618 + 0.5519 \ln(SSA) - 1.4495(SSA)^{-0.2640} \ln(T_{f,bulk} - T) \quad (3.10)$$

The soil's unfrozen water saturation, second approach, is determined by the volumetric unfrozen water content, taking into account the soil porosity (n), see Equation 3.11 [17].

$$S_{uw} = \frac{\theta_{uw}}{n} \quad (3.11)$$

The specific surface area (SSA) represents the total surface area of soil particles per

unit mass. This model is estimated using an empirical predictive power Equation 3.12 developed by Sepaskhah et al. (2010), which is defined based on the geometric mean of soil particle diameters [17].

$$SSA = 3.89 * d^{-0.905_g} \tag{3.12}$$

The geometric mean of soil particle diameter d_g is computed according to the findings of Shirazi and Boersma (1984), utilising the particle size boundaries outlined in the United States Department of Agriculture (USDA) soil classification system. It is assumed that there exists a lognormal distribution of particle sizes within these classification limits. The geometric mean of the soil particle diameter is defined as [17]:

$$d_g = exp(m_{cl} \ln d_{cl} + m_{si} \ln d_{si} + m_{sa} \ln d_{sa}) \tag{3.13}$$

Here m_{cl}, m_{si} and m_{sa} represent the mass fractions of clay, silt and sand respectively. The particle size limits according to the USDA soil classification system are defined in Table 3.2 [17].

Clay	d < 0.002 mm
Silt	$0.002 \leq d < 0.05mm$
Sand	$0.05 \leq d < 2.0mm$

Table 3.2: USDA classification limits for particle size

3.4 Elastic response

The elastic strains caused by stress in the solid phase can be determined using the shear modulus(G) and bulk modulus(K) of the soil, which are dependent on the equivalent stress. Refer to the following equations for the calculations, Equations 3.14 and 3.15 [17]:

$$G = (1 - S_{ice})G_0 + \frac{S_{ice}E_f}{2(1 + \nu_f)} \tag{3.14}$$

In this context:

- S_{ice} is the ice saturation
- G_0 is the soil shear modulus in an unfrozen state
- E_f is Young's modulus of frozen soil
- ν_f is the frozen Poisson's ratio

$$K = (1 - S_{ice})\frac{(1 + e)p*_{y0}}{\kappa_0} + \frac{S_{ice}E_f}{3(1 - 2\nu_f)} \tag{3.15}$$

In this context:

- e represents the soil void ratio
- $p*_{y0}$ is the pre-consolidation stress for unfrozen soil
- κ_0 is the elastic compressibility coefficient
- E_f is Young's modulus of frozen soil
- ν_f is the frozen Poisson's ratio

The ice saturation in a fully saturated soil can be determined using the following equation 3.16 [17]:

$$S_{ice} = 1 - S_{uw} \tag{3.16}$$

To account for the temperature-dependent behaviour of ice, the following expression is used for E_f:

$$E_f = E_{f,ref} - E_{f,inc}(T - T_{ref}) \tag{3.17}$$

Where

- $E_{f,ref}$ is Young's modulus of frozen soil at a reference temperature
- $E_{f,inc}$ is the rate at which Young's modulus changes with temperature
- T is the current temperature
- T_{ref} is the reference temperature

The formula adjusts Young's modulus (E_f) for frozen soil based on the current temperature relative to a reference temperature, using a linear relationship defined by $E_{f,inc}$. This allows for a more accurate representation of the soil's stiffness as it changes with temperature [17].

Because the mechanisms of pre-melting in frozen soil and capillary suction in unsaturated soil are similar, the elastic strain due to suction variation in frozen soil can be calculated using methods developed for unsaturated soils, such as those in the Barcelona Basic Model (BBM) [18].

$$d\epsilon^{se} = \frac{\kappa_s}{3(1+e)} \frac{ds_c}{(s_c + p_{at}} I \tag{3.18}$$

Where κ_s is the compressibility coefficient due to suction variation within the elastic region, s_c is the cryogenic suction, e is the void ratio, p_at is the atmospheric pressure, and I is the unit tensor [17].

3.5 Yield surfaces

For consistency, when cryogenic suction is zero, the model should transition to a standard unfrozen soil model. When cryogenic suction is zero, it implies that there is no freezing effect present. The soil behaves as it would under normal, unfrozen conditions. To maintain simplicity, the modified Cam-Clay model describes the behaviour of the unfrozen soil[17].

In the frozen state, the loading collapse (LC) yield surface is defined as a function of cryogenic suction s_c and unfrozen water saturation S_{uw}. The yield criterion for variations in the solid phase, F_1 is given by Equation 3.19.

$$F_1 = (p^* - k_t s_c)[(p^* - k_t s_c)S_{uw}^m - (p_y^* - k_t s_c)] + (\frac{q^*}{M})^2 \tag{3.19}$$

where

$$p^* *_y = p_c^*(\frac{q_{y0}^*}{p_c^*}^{\frac{\lambda_0 - \kappa}{\lambda - \kappa}} \tag{3.20}$$

$$\lambda = \lambda_0[(1-r)exp(-\beta s_c) + r] \tag{3.21}$$

$$\kappa = -\frac{1+e}{K} p_{y0}^* \tag{3.22}$$

The equation 3.19 provides a yield criterion for frozen soil, factoring in cryogenic suction and unfrozen water saturation to describe the conditions under which the soil will experience loading collapse [17].

To simulate the ice segregation phenomenon, the grain segregation (GS) yield criterion is adopted for suction-induced plastic deformation, and Equation 3.23 applies [17].

$$F_2 = s_c - s_{c,seg} = 0 \tag{3.23}$$

3.6 Hardening rules

Plastic compression from changes in solid phase stress results in a stiffer soil behaviour, causing the LC yield surface to expand outward. Additionally, this compression reduces void dimensions, leading to a lower segregation threshold. This behaviour can be modelled using a coupled hardening rule (Equation 3.24), which shifts the GS yield surface downward [17].

$$\frac{dp_{yo}^*}{p_{y0}^*} = \frac{1+e}{\lambda_0 - \kappa_0} d\epsilon_v^{mp} + \frac{1+e}{\lambda_0 - \kappa_0} d\epsilon_v^{sp} \tag{3.24}$$

Plastic dilation caused by ice segregation results in an upward shift of the GS yield surface and a softer soil behaviour, leading to the inward movement of the LC yield surface. Equation 3.25 gives the hardening rule for the GS yield surface [17].

$$\frac{ds_{s,seg}}{s_{s,seg} + p_{at}} = -\frac{1+e}{S_{uw}(\lambda_s + \kappa_s)} d\epsilon_v^{sp} - \frac{1+e}{\lambda_s + \kappa_s}(1 - \frac{S_c}{S_{s,seg}}) d\epsilon_v^{mp} \tag{3.25}$$

3.7 Flow rules

Different flow rules are used for the LC and GS yield surfaces to describe their respective plastic deformation behaviours, with the plastic potential function Q_1 providing additional detail on the deformation direction. A non-associated flow rule is applied to the LC yield surface (Equation 3.26), whereas an associated flow rule is used for the GS yield surface (Equation 3.27). The plastic potential function Q_1 is provided in Equation 3.28 [17].

$$d\epsilon^{mp} = d\lambda_1 \frac{\delta Q_1}{\delta \sigma^*} \tag{3.26}$$

$$d\epsilon^{sp} = d\lambda_2 \frac{\delta F_2}{\delta s_c} I \tag{3.27}$$

$$Q_1 = S_{uw}^{\gamma}(p^* - \frac{p_y^* + k_t s_c}{2})^2 + (\frac{q^*}{M})^2 \tag{3.28}$$

3.8 Model parameters

There are three kinds of input parameters in this model:

- The soil parameters
- The parameters for initialising the state variables
- The ice and water parameters

In Figure 3.2 the parameters are summarized in which kind of input each parameter locates [17].

Soil parameters	T_{ref}	$E_{f,ref}$	$E_{f,inc}$	ν_f	G_0	κ_0	p_c^*	λ_0	
	γ	k_t	M	λ_s	κ_s	r	β	m	p_{at}
Parameters for initialising the state variables	$\left(p_{y0}^*\right)_{in}$	λ_r	Y_{ref}	Δp_{y0}^*	e_0	$(s_{c,seg})_{in}$			
Ice and water parameters	ρ_r	α	T_{ref}	p_{ref}	K_w				

Figure 3.2: Input model parameters

Conducting an unconfined triaxial compression test on soil in its frozen state at a specific reference temperature allows for the determination of the reference Young's modulus of the frozen soil, $E_{f,ref}$. Performing a similar test at a different sub-zero temperature can be used to find $E_{f,inc}$, which explains the increase in soil stiffness with decreasing temperature. Table 3.3 presents default values by model developers [17].

The Poission's ratio of ice, ν_{ice}, is approximately 0.31. It is suggested by the model developers to use a value of ν_f that is close to ν_{ice}, using Equation 3.15. The Poission's ratio in the model is assumed to be constant for frozen soil [9].

Pressure dependence is managed using the parameters G_0 and κ_0. The shear modulus (G_0) of unfrozen soil is determined through a simple shear test in its unfrozen

Soil parameters	Frozen sand	Frozen silt	Frozen clay
$E_{f,ref}$ [MPa]	500	400	500
$E_{f,inc}$ [MPa/K]	2100	1400	230

Table 3.3: Default values of elastic parameters

state. The elastic compressibility coefficient of frozen soil (κ_0) is obtained from an unfrozen oedometer test [17].

The parameter κ_s describes the elasticity dependent on suction, representing the compressibility coefficient for changes in suction. The model developers recommend determining it using a suction-controlled frost heave test [17].

The parameter ($s_{c,segin}$) is the initial value of grain segregation threshold derived from suction-controlled frost heave test. It describes the limit after which both elastic and plastic strains occur with increasing cryogenic suction [17].

$$(s_{c,segin}) \approx |T_{f,bulk} - T| X \frac{MPa}{K} \tag{3.29}$$

The initial threshold value for grain segregation ($s_{c,segin}$) is approximated based on Rempel (2007) by use of Equation 3.29. The proposed default values when no frost heave test has been performed are [17]:

- 0.55 MPa for sand
- 1.25 MPa for silt
- 3.50 MPa for clay

A drained simple shear strength test on soil in its unfrozen state can be used to determine both the elastic shear modulus, G_0, and the slope of the critical state line, M. M represents the slope of the critical state line, which describes a condition of no volumetric deformation during shear. This slope is determined using a simple shear test in the unfrozen state and is assumed to be constant for unfrozen soil [17].

In the F-u model interfaces, ϕ' denotes the friction angle at the critical state during triaxial compression. The friction angle ϕ' can be expressed as a function of M as follows [17]:

$$\sin(\phi') = \frac{3M}{6 + M} \tag{3.30}$$

Here, M was assigned a value of 1.2. Then, ϕ' is determined by rearranging Equation 3.30. Which results in $\phi' = 30$.

Parameter κ_t is the increment in apparent cohesion due to cryogenic suction, which is assessed by comparing cohesion values from unconfined axial compression tests conducted at varying freezing temperatures. Parameters m and γ are parameters used to adjust the impact of unthawed water saturation on the LC yield surface F_1 and plastic potential function Q_1 respectively [17].

Parameters λ_0 and λ_s are elastoplastic compression coefficients for unfrozen soils and suction variation. They are derived from an unfrozen oedometer test and suction-controlled frost heave tests [17].

Parameter $(p^*_{y0})_{in}$ is the initial preconsolidation stress in unfrozen condition at reference depth Y_{ref} that is suggested to be defined from unfrozen oedometer tests. The change of preconsoldation stress with depth is represented by parameter Δp^*_{y0} [17].

Parameter β controls the rate of change in soil stiffness with suction variation. Parameter r is a coefficient for maximum soil stiffness. Parameter p^*_c is the soil reference stress. These parameters are suggested to be estimated from oedometer tests at different constant positive and negative temperatures using the calibration process adapted by the model authors from the work of Zhang et al. (2016) [19].

4

Methods

4.1 Soil properties and geometry

For this report, the geotechnical parameters were primarily evaluated using cone penetration tests (CPTs) analyzed through the software Conrad. Parameters not obtained from data were either estimated or assigned default values as specified in the model manual [5].

The site used for reference lies between the village of Bispgården and the former rapids, Döda Fallet, in Jämtland County, Sweden. The top 10 meters of soil were assessed through CPTs revealing a composition of numerous, often very thin layers of sand, silt, or clay. A consistent characteristic among these layers is their relatively high silt content, rendering them susceptible to frost and erosion [5].

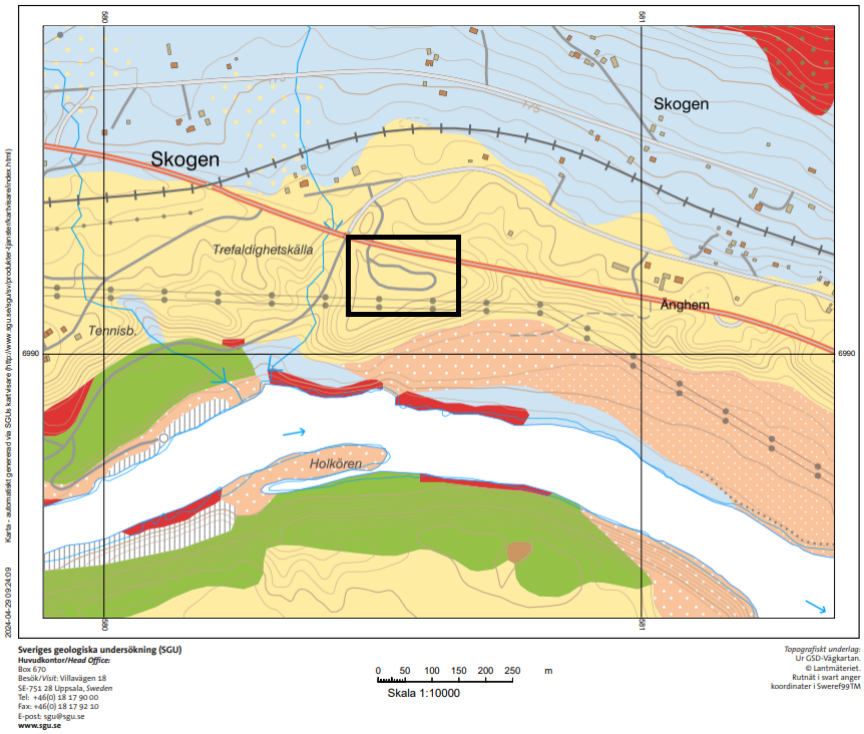

Figure 4.1: Soil Type Overview with Demonstration Trial Areas Marked in Black [12]

The soil type map from the Geological Survey of Sweden (SGU) indicates a composition ranging from clay to silt in the topsoil, see Figure 4.1. Notably, the soil at Bispgården exhibited a much finer texture compared to the test soil, prompting adjustments to the parameters. However, the accuracy of these modifications was constrained by available data and modelling constraints, leading to an iterative process of balancing desired parameters with feasible ones [5].

The model's height was designated as 15 meters, featuring a 30° inclined slope that extended 5 meters further downward. To simplify the geometry, the length was constrained to 15 meters horizontally backwards from the top and 15 meters horizontally forward from the toe of the slope, as illustrated in Figure 4.2 [5].

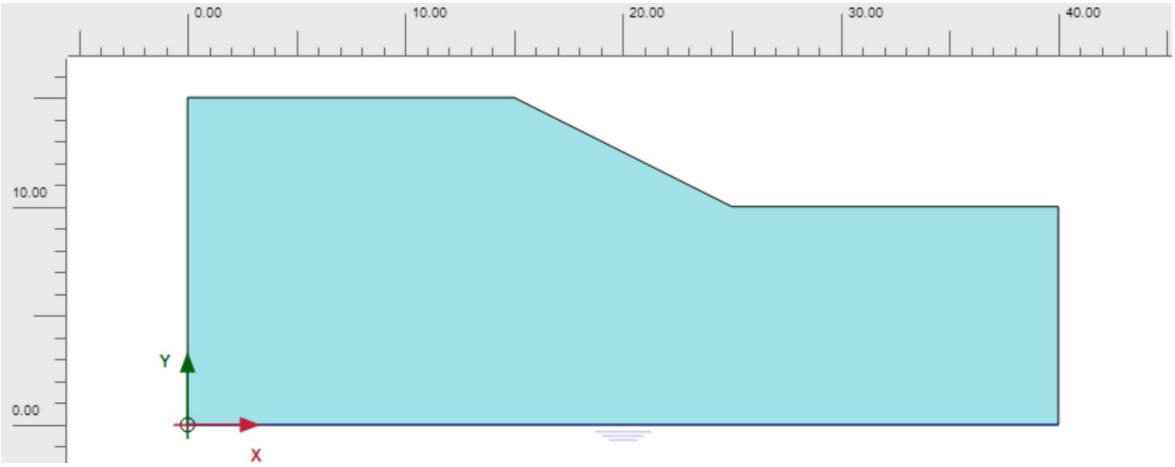

Figure 4.2: A profile of the slope

Three nodes were selected along the surface of the slope. See Figure 4.3.

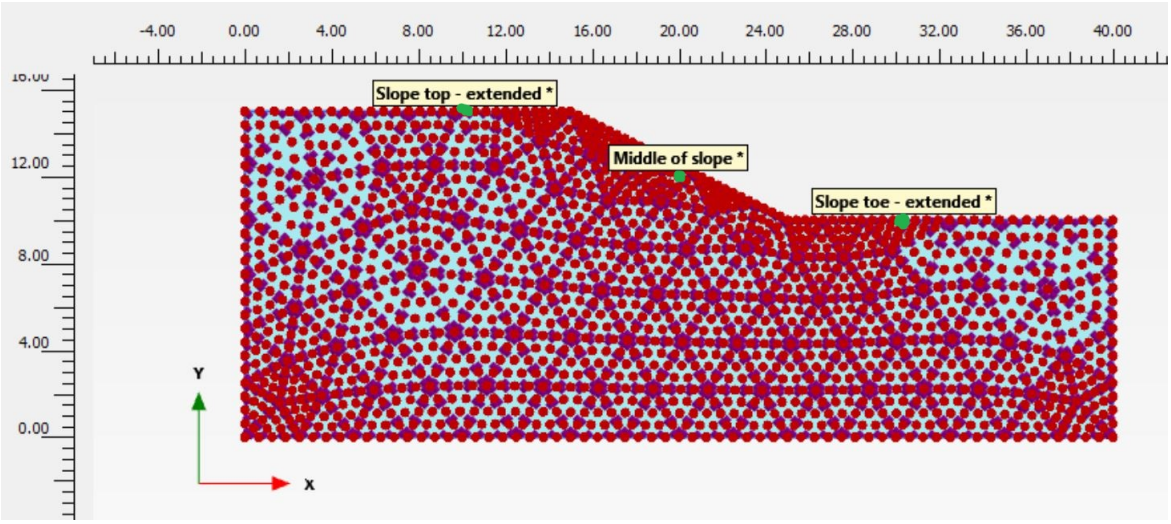

Figure 4.3: A profile of the slope with selected nodes.

A slope with identical geometry was used for both the test model and the frozen-unfrozen (FU) model to simulate the freeze-thaw cycle. The material was deemed

sufficiently homogeneous to be represented as a single layer, and due to the complexities of the FU model, the findings were consolidated into this single material [5]. The soil properties for the test model are detailed in Table A.1. Table A.2 refers to parameters involved with water and ice in both models. While the soil properties for the FU model are provided in Table A.3 and Table A.4.

4.2 Climate in the region of Jämtland

As previously mentioned, the slope geometry and material are based on a different project situated in the Jämtland region of Sweden. The climate conditions for this project were thoroughly researched and documented in a report by Nylen et al. (2015). The study details both current and projected climate conditions in Jämtland, utilizing observational data and climate modelling insights [7].

To replicate the temperature variations experienced during seasonal changes, two temperature functions were developed, as outlined in Tables B.1 and B.2. The first function simulates the thawing period, transitioning from frozen soil to thawed soil, while the second function simulates the freezing period, transitioning from thawed soil to frozen soil.

4.3 Test model

A test model was designed to increase knowledge about the effects of thermal influence in soil and the influence of various boundary conditions on analysis. This model is unrelated to the frozen and unfrozen models talked about later on. The main goal of the test model was to investigate the processes of freezing and thawing in the soil with the use of PLAXIS 2D. The test model was based on a linear elastic framework. The elastic model was configured to be drained, moderately fine and an-isotropic.

4.3.1 Boundary conditions

A thermal flow line was introduced at the top of the slope. The thermal inflow at the top was left open, alongside the seepage. This setup enabled a thorough analysis of how thermal energy moves through the soil and water, particularly at the interface between the soil surface and the surrounding air temperature. Conversely, the bottom boundary was sealed off for thermal inflow and seepage. Additionally, the slope's side and bottom were closed off for thermal inflow also one side was closed to seepage and the other one was set as open, see Figures 4.4 and 4.5.

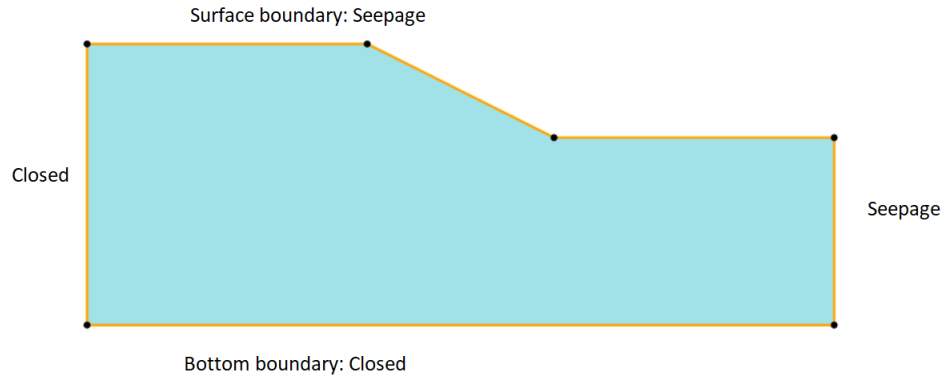

Figure 4.4: Selected boundary conditions for water flow

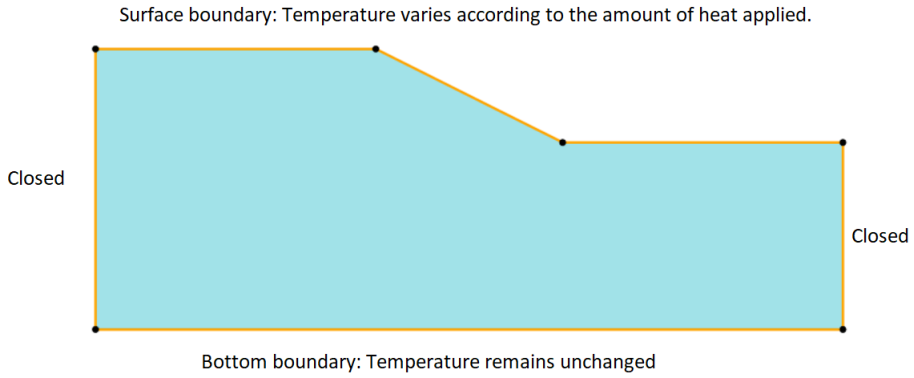

Figure 4.5: Selected boundary conditions for thermal flow

4.3.2 Scenarios

As mentioned previously there are two different boundary conditions assigned to the model. Firstly, the climate-based conditions are set to stimulate real-life climate data in the area. It is assumed that the primary driver of change is the surface transfer parameter. In this model, three distinct surface transfer values are individually assigned: $1W/m^2/K$, $5W/m^2/K$, and $10W/m^2/K$. The surface transfer parameter measures how quickly energy moves between the soil surface and the air. Refer to Table B.1 and Table B.2 for two distinct periods: one simulates a thawing period, while the other simulates a freezing period. The other boundary conditions involve how water moves through the soil, this is set as seepage. There is now precipitation assigned to the model but a groundwater line is set at the bottom boundary.

4.4 The Frozen and Unfrozen Model

The freezing and thawing of the soil were simulated using finite element analysis, utilizing the Frozen and Unfrozen soil model developed by Ghoreishian Amiri et al. (2016), which was initially created by the Norwegian University of Science and Technology and PLAXIS 2d, and later enhanced by Aukenthaler (2015). The processes have been previously described in Chapter 3.

The ice saturation curve incorporated in the PLAXIS model functions as a critical parameter governing the soil's freezing and thawing processes. This curve illustrates the relationship between the degree of ice saturation within the soil pores and the corresponding temperature conditions. Its integration into the model enables the simulation of how the soil's moisture content evolves with fluctuating temperatures, particularly during freezing and thawing events. The ice saturation curve was assigned to represent a northern atmosphere, see Figure 4.6.

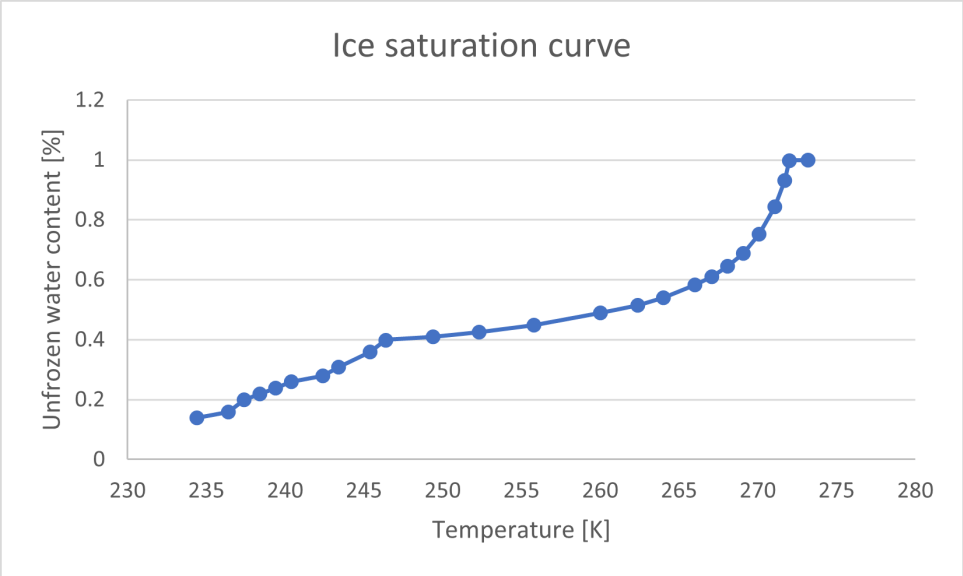

Figure 4.6: Assigned ice saturation curve

4.4.1 Boundary conditions

Located in Northern Sweden, Bispgården experiences a subarctic climate characterized by its long, icy winters and short, mild summers. Temperature variations are notable throughout the year. The warmest months, typically June, July, and August, feature average temperatures ranging from 10 to 20°C. In contrast, the coldest months, namely December, January, and February, often see temperatures dropping considerably below freezing, averaging around -15 to -5°C [7]. As previously mentioned, temperature functions were established in the test model to replicate these temperature variations; these functions were also applied to the FU model with the appropriate boundary conditions for the climate. Refer to B.1 and B.2 in Appendix B for details. Similar to the test model, in this model, three distinct surface transfer

values are assigned individually as in the Test model:

- $1W/m^2/K$
- $5W/m^2/K$
- $10W/m^2/K$

Two additional temperature functions were also assigned, see Tables B.4 and B.3. They were assigned to simulate thermal flow in the soil. The temperature functions were assigned on the surface boundary and assumed to move within the soil due to gravity and other forces.

It is assumed that the lower boundaries remain constant at a temperature of 273.15 K, and no precipitation is expected to reach this level. Instead, the movement of water is presumed to occur solely due to gravity. See Figure 4.4. The temperature at the upper boundaries was adjusted over time to simulate weather changes throughout the freeze-thaw cycle (FTC).

Two distinct sets of boundary conditions were established for the FU model at the slope surface. Initially, the climate boundary conditions utilized the air temperature above the soil to regulate the surface temperature of the slope, see Figure 4.5. Subsequently, thermal flow boundary conditions were applied as outlined in the test model description, see Figure 4.5. The analysis was executed spanning 150 days under both sets of boundary conditions.

4.5 Calculating the Safety Factor

The computed finite element stresses can then be imported into a conventional limit equilibrium analysis. The stresses σ_x, σ_y, and τ_{xy} within each element allow for the computation of normal and mobilized shear stresses at the base midpoint of each slice. This process involves projecting the known stresses at the Gauss numerical integration point in each element to the nodes, averaging them at each node, and subsequently computing the stresses at any other point within the element [13].

Furthermore, we can compute the slice base normal and shear stress using ordinary Mohr circle techniques, determine the available shear strength for the computed normal stress, and multiply the mobilized shear and available strength by the length of the slice base to convert stress into forces. This process is repeated for each slice successively up to slice number n [13].

Once the mobilized and resisting shear forces are available for each slice, they can be integrated over the length of the slip surface to ascertain a stability factor. This

factor, represented as

$$S.F = \frac{\sum S_r}{\sum S_m} \tag{4.1}$$

is defined as the summation of the total available shear resistance (S_r) over the total mobilized shear (S_m) along the entire length of the slip surface. Others have presented similar expressions for stability factors [13].

In this analysis, SF was calculated using both a Python tool and manually with Excel. The SF calculation was applied only after analyzing the FU model. It was deemed unnecessary for the test model, as the primary objective of the test model was to understand the different boundary conditions affecting the evaluated slope.

The Python tool was more thorough as it evaluated multiple slip surfaces, specifically six different ones, and used more point along the slip surfaces. The results from the Python code provided the minimum SF, the critical points (x_c, y_c), and the radius, R.

4.5.1 Estimating the slip surface

In this analysis, AutoCAD was employed to draw the coordinates of the slope and to create a circle above the slope to estimate its slip surface, see Figure 4.7. The radius of this circle is represented by R, while the critical points of the circle are denoted as x_c and y_c. Once the slip surface was estimated, it was divided into slices and points along the slip surface were assigned. As described in Chapter 2.4, which discusses the calculation of the safety factor using the ordinary method. After the slices were defined, the length of each slice was measured. Additionally, each slice had a θ value that was estimated, along with the coordinates of the slice's locations on the slope. See Figure 4.8.

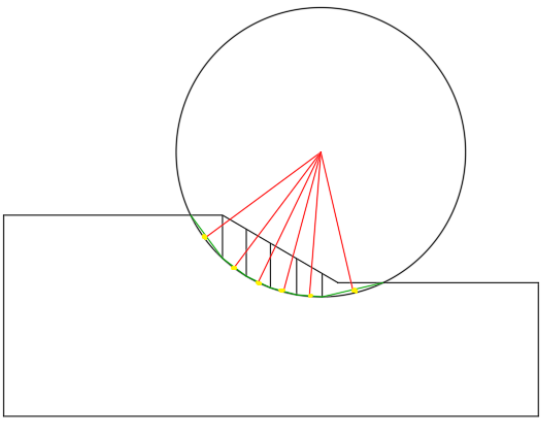

Figure 4.7: Estimating the slip surface for the Bispgården slope

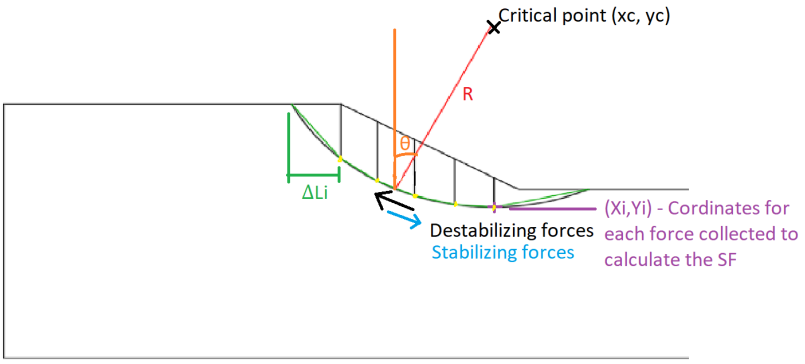

Figure 4.8: Explanations on how parameters for the SF calculations were extracted

The stability forces in the slope are determined using estimated values of the effective cohesion c' and the effective angle of internal friction ϕ'. These parameters are used in Equation 4.2 to find the normal stress σ'_{ni} acting on each slice.
Here σ'_{xx} and σ'_{yy} are the normal stresses in the x and y directions, respectively, and τ_{xy} is the shear stress. θ represents the angle of the slice relative to a reference direction.

$$\sigma'_{ni} = \frac{\sigma'_{xx} + \sigma'_{yy}}{2} + \frac{\sigma'_{xx} - \sigma'_{yy}}{2} cos(2\theta) + \tau_{xy} sin(2\theta) \tag{4.2}$$

The shear stress, $\tau_{shear,i}$, on each slice can be calculated using Equation 4.3

$$\tau_{shear,i} = -\frac{(\sigma'_{xx} + \sigma'_{yy})}{2} sin(2\theta) + \tau_{xy} cos(2\theta) \tag{4.3}$$

Finally, the safety factor (SF) is calculated by comparing the resisting forces to the driving forces along the slip surface. The formula for the safety factor is given by:

$$SF = \frac{\sum_{i=1}^{n} (c' + \sigma'_{ni} + tan(\phi')) * \Delta L_i}{\sum_{i=1}^{n} \tau_{shear,i}} \tag{4.4}$$

In this equation:

- c' is the effective cohesion
- σ'_{ni} is the normal stress acting on the slice
- $tan(\phi')$ is the tangent of the effective angle of internal frictions
- ΔL_i is the length of the slice
- $\tau_{shear,i}$ is the shear stress acting on the slice

The summation is carried out over all slices i from 1 to n. This approach allows for the estimation of the slope's stability by integrating the effects of both normal and shear stresses on the potential slip surface.

5
Results

5.1 Test model

These are the results of the test model discussed earlier, in which temperature changes were applied as loads on the surface. Where the various surface transfers were examined and observed for their impact. Greater surface transfer results in a more significant temperature variation. This was primarily observed at the top slope node. The node representing the midpoint of the slope remains stable during both the thawing and freezing of the soil.

5.1.1 Heat analysis

5.1.1.1 Scenario: Summer to Autumn

Start by looking at the summer-to-autumn scenario with a surface transfer of $1w/m^2/K$. Figure 5.1 shows how the temperature is distributed over a period of time, the time was set to be 150 days.

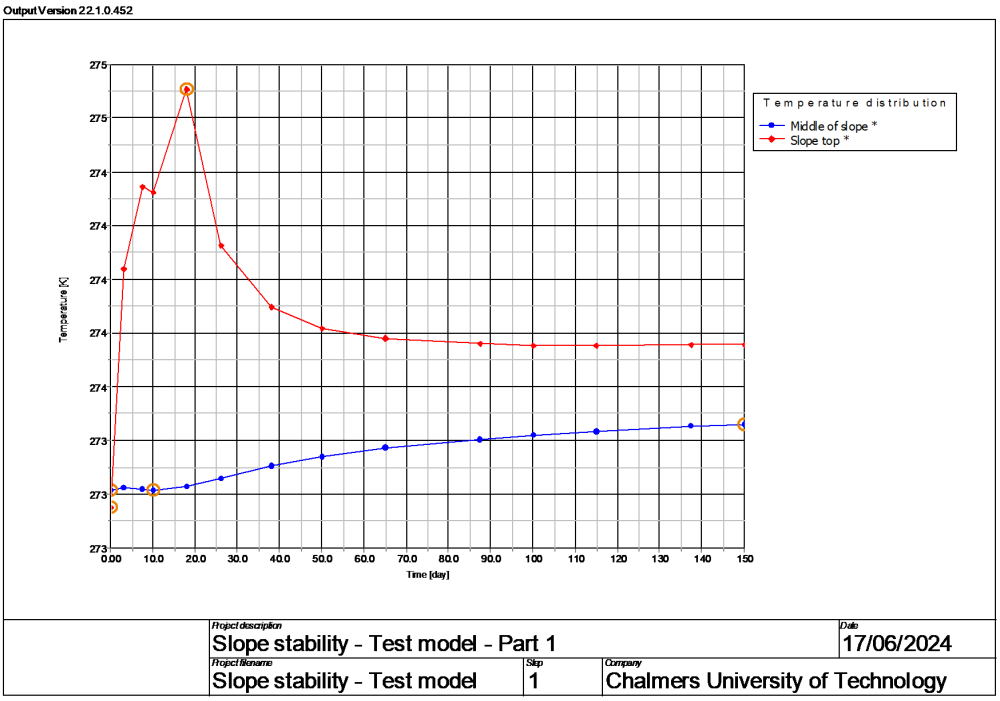

Figure 5.1: Temperature distribution for the test model for summer to autumn with $1W/m^2/K$

Figure 5.2 shows how the temperature is distributed over a period of time, the time was set to be 150 days.

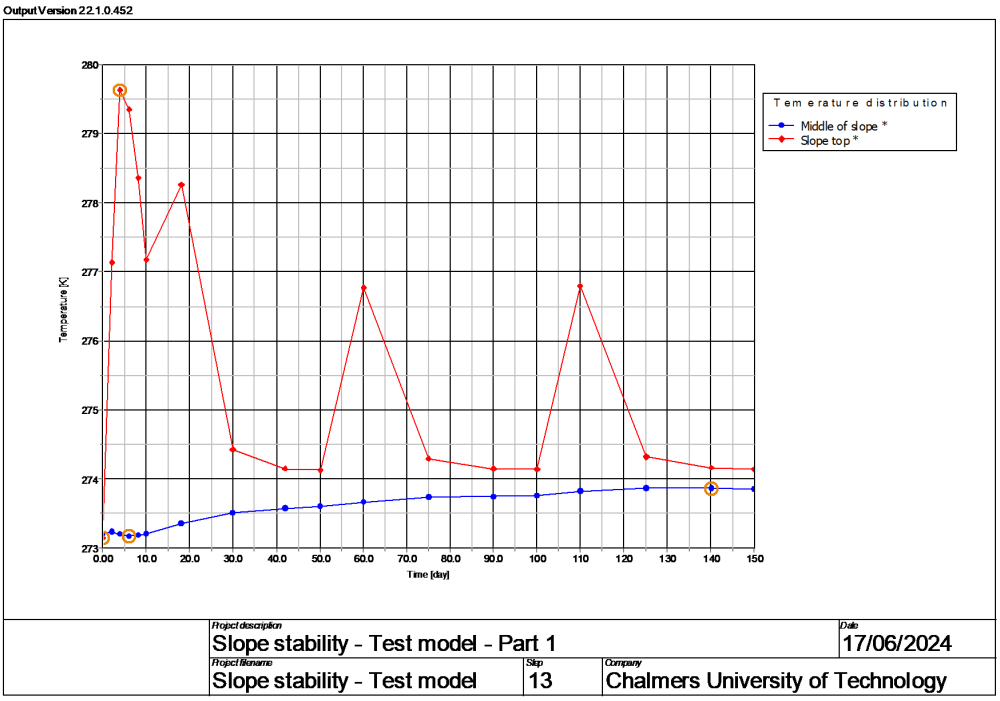

Figure 5.2: Temperature distribution for the test model for summer to autumn with $5W/m^2/K$

Figure 5.3 shows how the temperature is distributed over a period of time, the time was set to be 150 days.

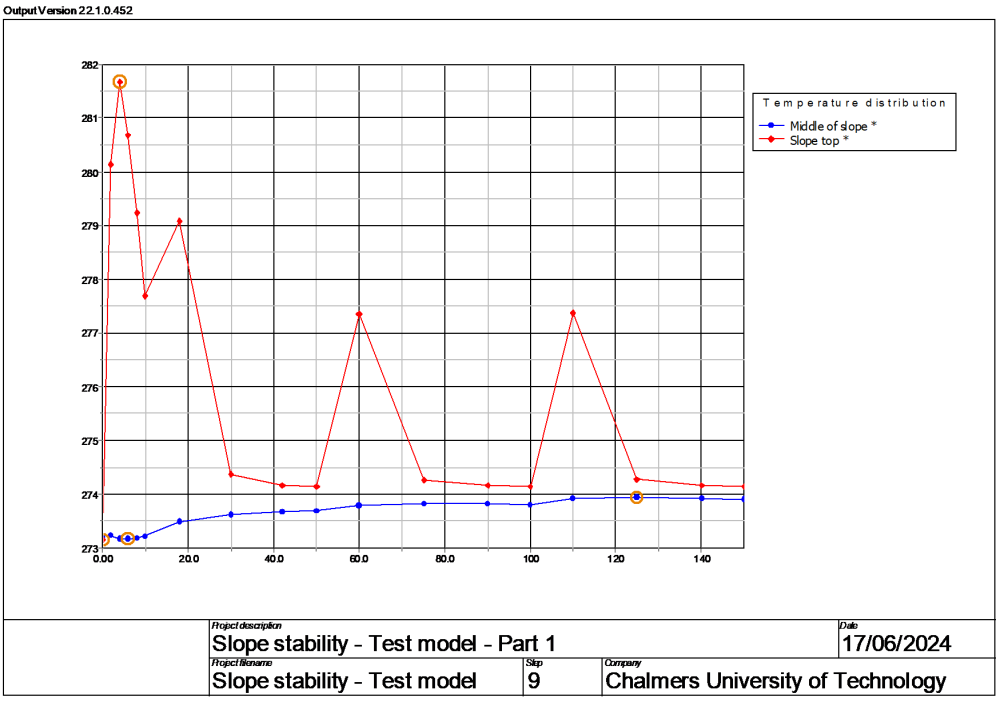

Figure 5.3: Temperature distribution for the test model for summer to autumn with $10W/m^2/K$

5.1.1.2 Scenario: Winter to spring

Next, look at the winter-to-spring scenario with a surface transfer of $1w/m^2/K$. See Figure 5.4.

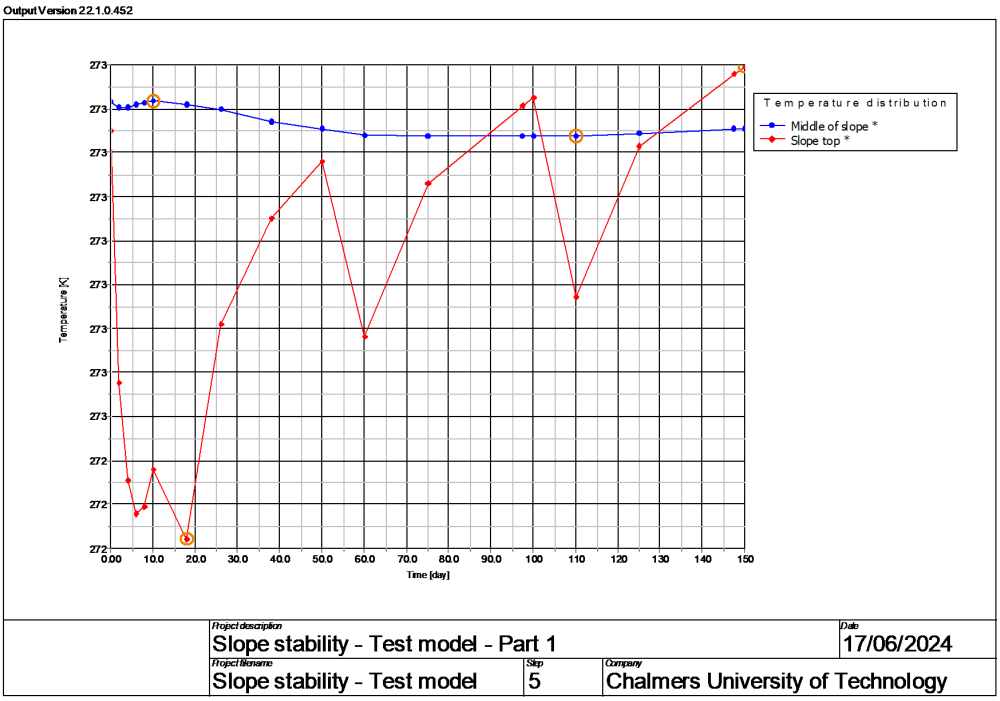

Figure 5.4: Temperature distribution for the test model for winter to spring with $1W/m^2/K$

Next, look at the winter-to-spring scenario with a surface transfer of $5w/m^2/K$. See Figure 5.5.

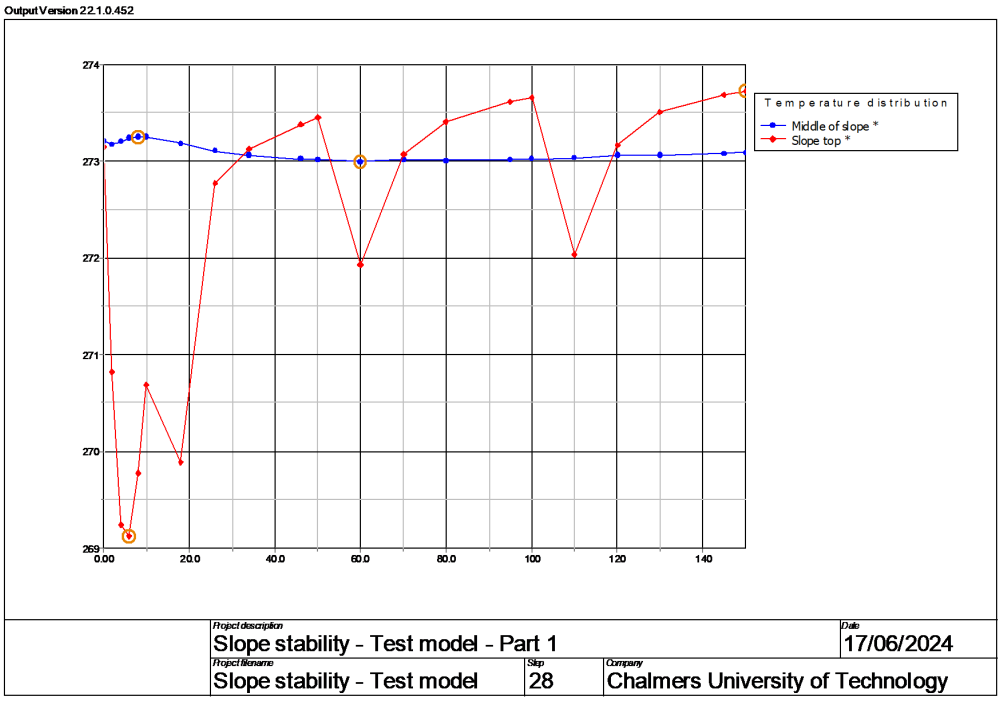

Figure 5.5: Temperature distribution for the test model for winter to spring with $5W/m^2/K$

Next, look at the winter-to-spring scenario with a surface transfer of $10w/m^2/K$. See Figure 5.6.

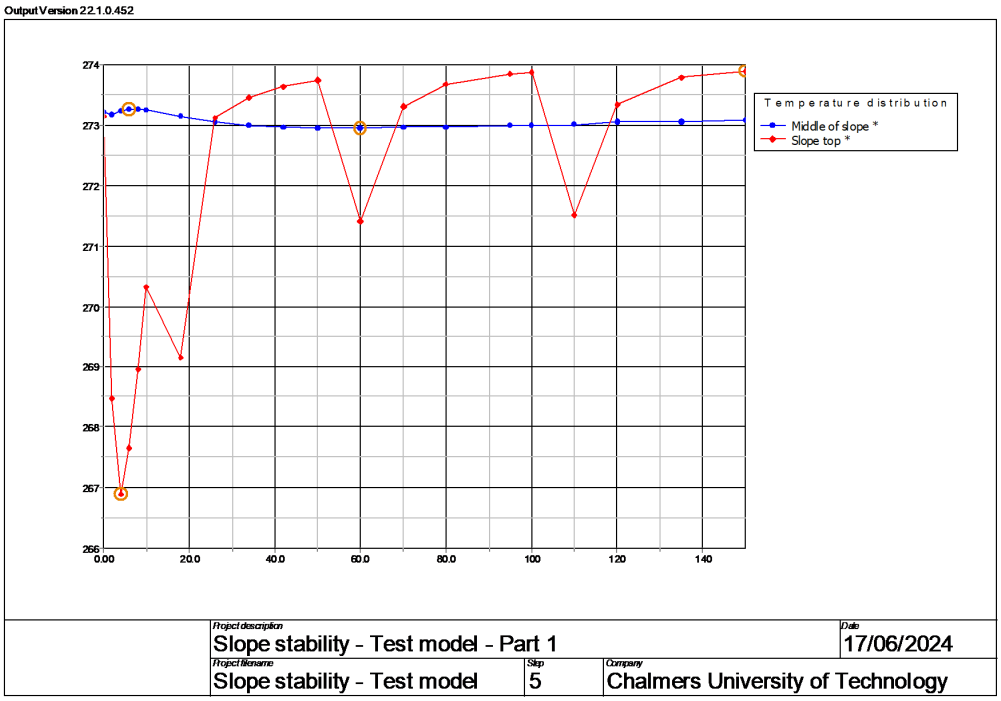

Figure 5.6: Temperature distribution for the test model for winter to spring with $10 W/m^2/K$

5.2 Frozen and unfrozen model

The results from the FU model in PLAXIS. The first set of results is based on boundary conditions derived from the climate of the Jämtland region. The second set is based on an assigned thermal flow in the soil, which does not include climate data but relies solely on knowledge of thermal flow behaviour in cold regions.

5.2.1 Climate based conditions

5.2.1.1 Temperature distribution

A profile of the temperature fluctuations is illustrated in Figure 5.7. The figure shows how the climate condition boundaries affect the temperature, considering a surface transfer rate of $1 W/m^2/K$ and freezing behaviour in the climate.

For the first 20 days, the maximum temperature is 273.2 K and the minimum temperature is 271.4 K. For the next 30 days, or by day 50, the minimum temperature drops to 270.5 K while the maximum temperature remains the same as in the previous phase. During the next 50 days, the maximum temperature decreases to 273.1 K and the minimum temperature falls to 269.2 K. In the last phase of the model, by day 150, the maximum temperature remains the same as in the previous phase, and the minimum temperature decreases further to 268.5 K.

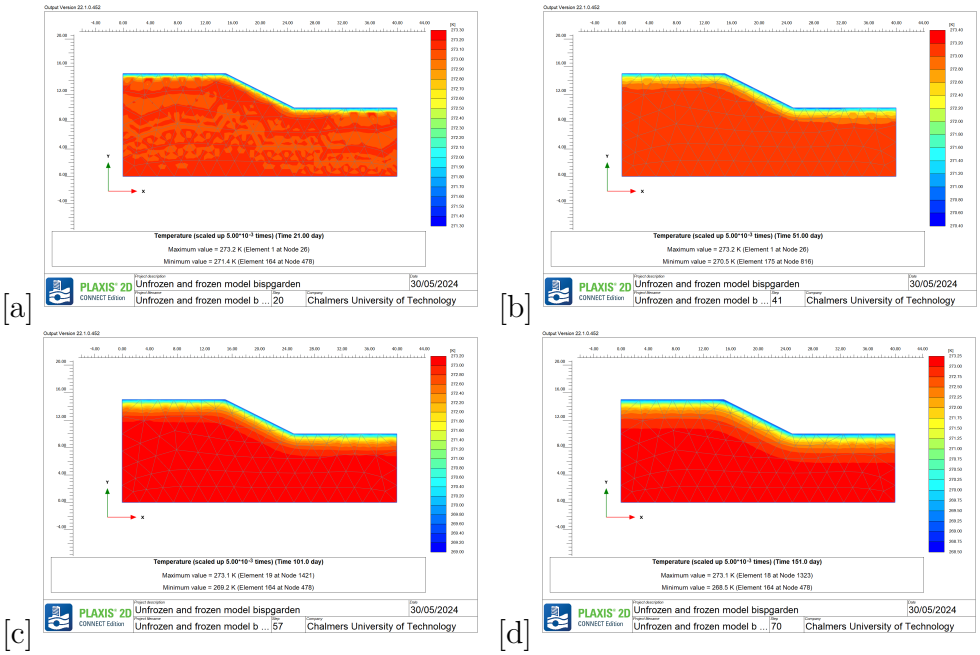

Figure 5.7: Profile of the temperature distribution when climate is freezing and surface transfer is $1W/m^2/K$ for (a) 20 days (b) 50 days (c) 100 days (d) 150 days

Additionally, figure 5.8 illustrates the temperature distribution over time with three designated nodes. The locations of these nodes are depicted in Figure 4.3. All three points exhibit similar behaviour.

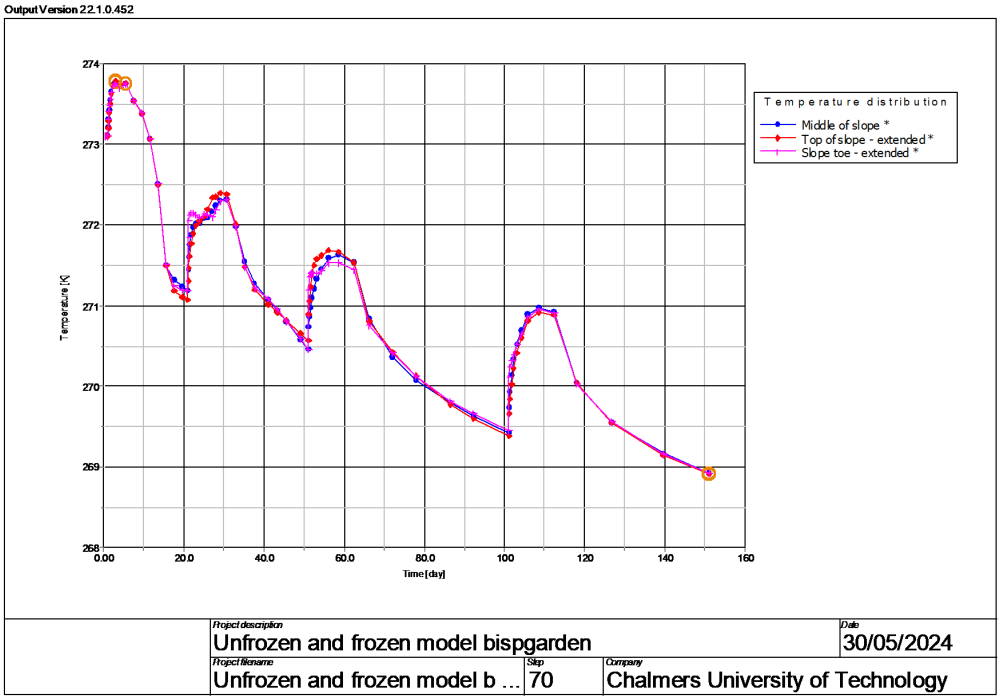

Figure 5.8: Temperature distribution when climate is freezing and surface transfer is $1W/m^2/K$

A profile of the temperature fluctuations is illustrated in Figure 5.9. The figure shows how the climate condition boundaries affect the temperature, considering a surface transfer rate of $5W/m^2/K$ and freezing behaviour in the climate.

For the first 20 days, the maximum temperature is 274.0 K and the minimum temperature is 268.3 K. For the next 30 days, or by day 50, the minimum temperature drops to 266.3 K alongside the maximum temperature which drops to 273.3 K from the previous phase. During the next 50 days, the maximum temperature decreases to 273.1 K and the minimum temperature falls to 264.9 K. In the last phase of the model, by day 150, the maximum temperature remains the same as in the previous phase, and the minimum temperature decreases further to 264.6 K.

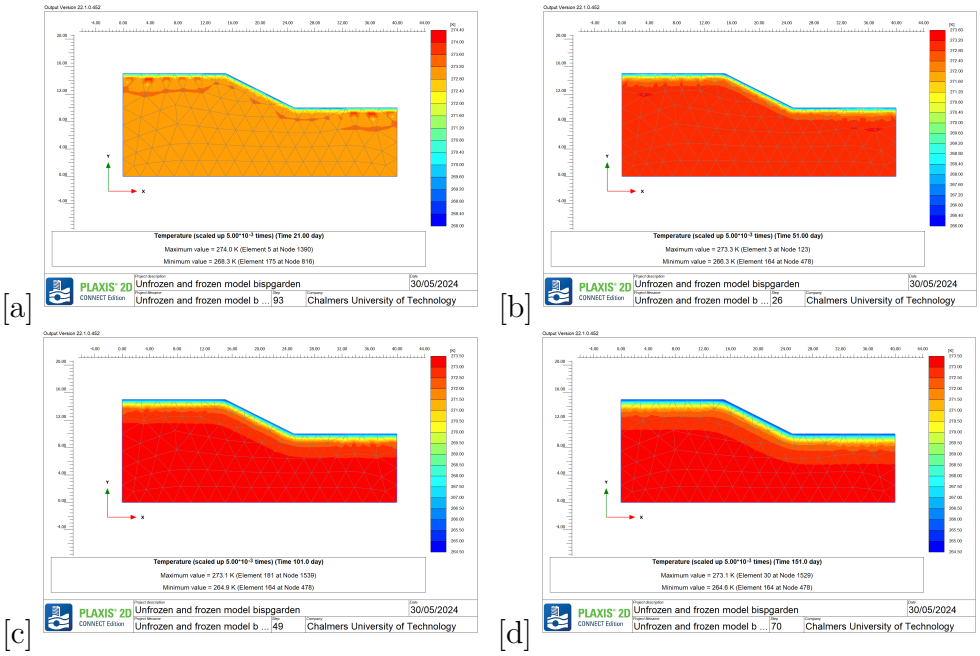

Figure 5.9: Profile of the temperature distribution when climate is freezing and surface transfer is $5W/m^2/K$ (a) 20 days (b) 50 days (c) 100 days (d) 150 days

Additionally, figure 5.10 illustrates the temperature distribution over time with three designated nodes. The locations of these nodes are depicted in Figure 4.3. All three points exhibit similar behaviour.

A profile of the temperature fluctuations is illustrated in Figure 5.11. The figure shows how the climate condition boundaries affect the temperature, considering a surface transfer rate of $10W/m^2/K$ and freezing behaviour in the climate.

For the first 20 days, the maximum temperature is 274.2 K and the minimum temperature is 266.3 K. For the next 30 days, or by day 50, the minimum temperature drops to 264.8 K alongside the maximum temperature which drops to 273.3 K from the previous phase. During the next 50 days, the maximum temperature decreases to 273.1 K and the minimum temperature falls to 263.9 K. In the last phase of the

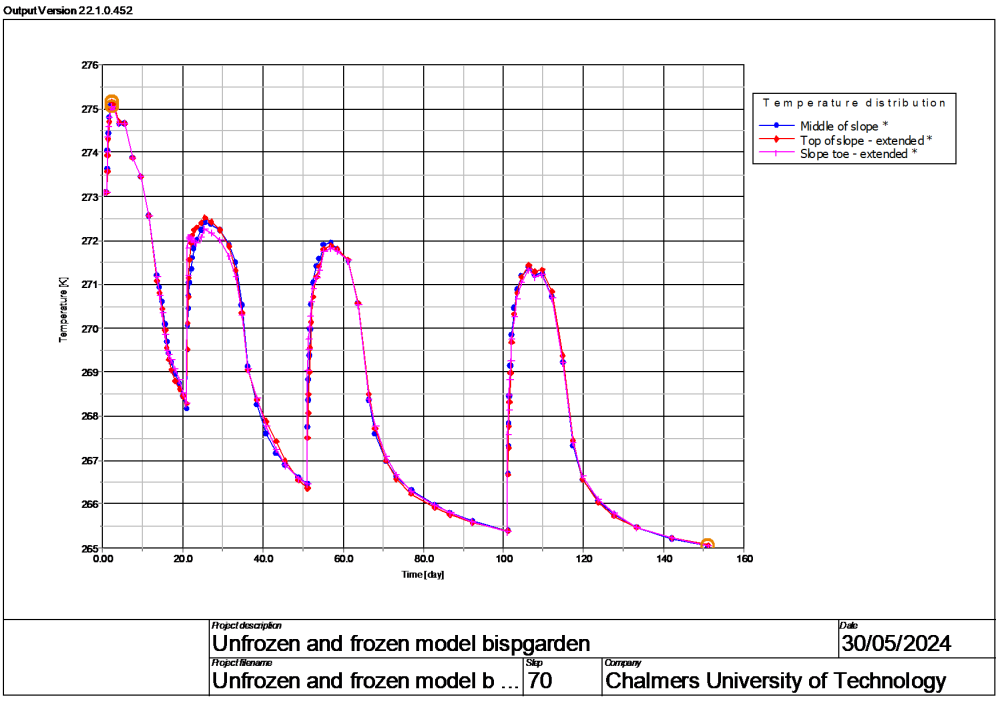

Figure 5.10: Temperature distribution when climate is freezing and surface transfer is $5W/m^2/K$

model, by day 150, the maximum temperature remains the same as in the previous phase, and the minimum temperature decreases further to 263.7 K.

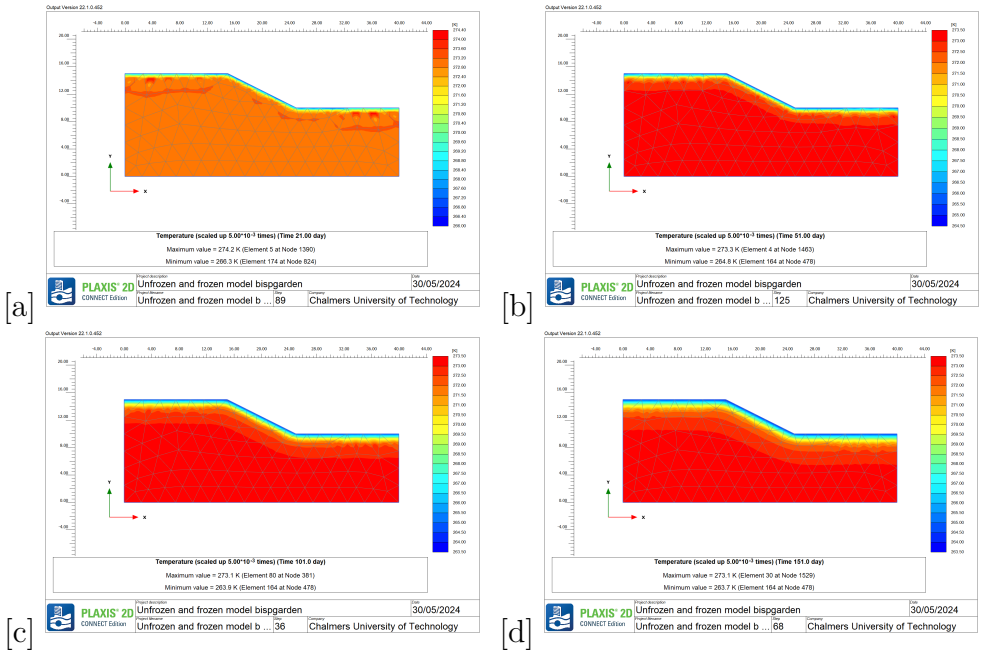

Figure 5.11: Profile of the temperature distribution when climate is freezing and surface transfer is $10W/m^2/K$ (a) 20 days (b) 50 days (c) 100 days (d) 150 days

Additionally, figure 5.12 illustrates the temperature distribution over time with three designated nodes. The locations of these nodes are depicted in Figure 4.3. All three points exhibit similar behaviour.

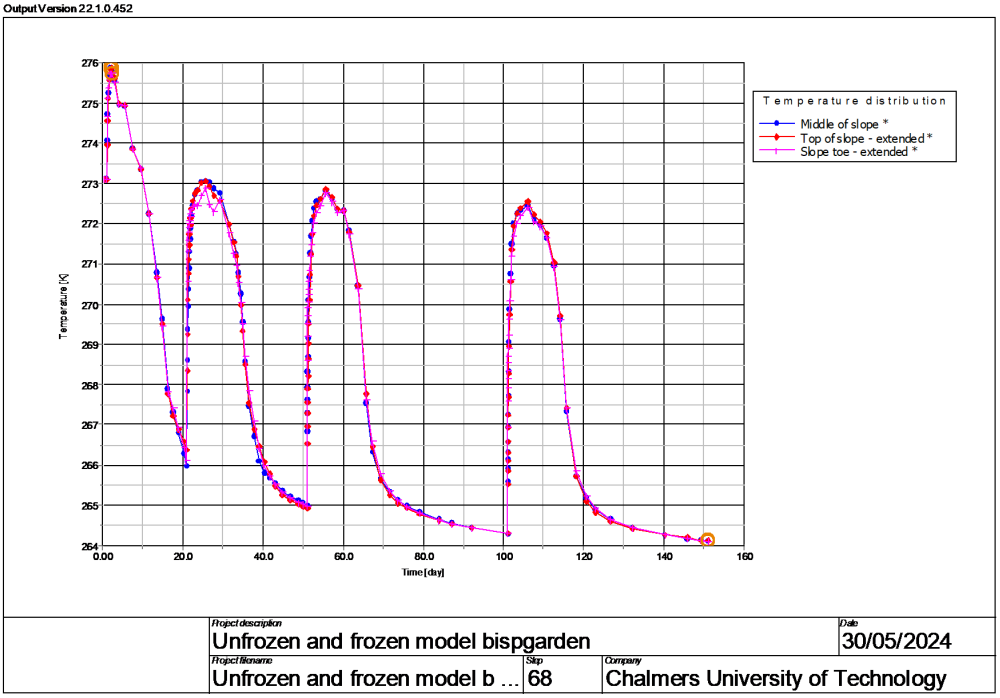

Figure 5.12: Temperature distribution when climate is freezing and surface transfer is $10W/m^2/K$

A profile of the temperature fluctuations is illustrated in Figure 5.13. The figure shows how the climate condition boundaries affect the temperature, considering a surface transfer rate of $1W/m^2/K$ and thawing behaviour in the climate.

For the first 20 days, the maximum temperature is 273.1 K and the minimum temperature is 271.8 K. For the next 30 days, up to day 50, both the maximum and minimum temperatures remain the same as in the previous phase. Over the subsequent 50 days, the maximum temperature stays consistent with the previous phases, while the minimum temperature increases to 272.1 K. In the final phase of the model, by day 150, the maximum temperature remains unchanged, and the minimum temperature rises further to 272.2 K.

Additionally, figure 5.14 illustrates the temperature distribution over time with three designated nodes. The locations of these nodes are depicted in Figure 4.3. All three points exhibit similar behaviour.

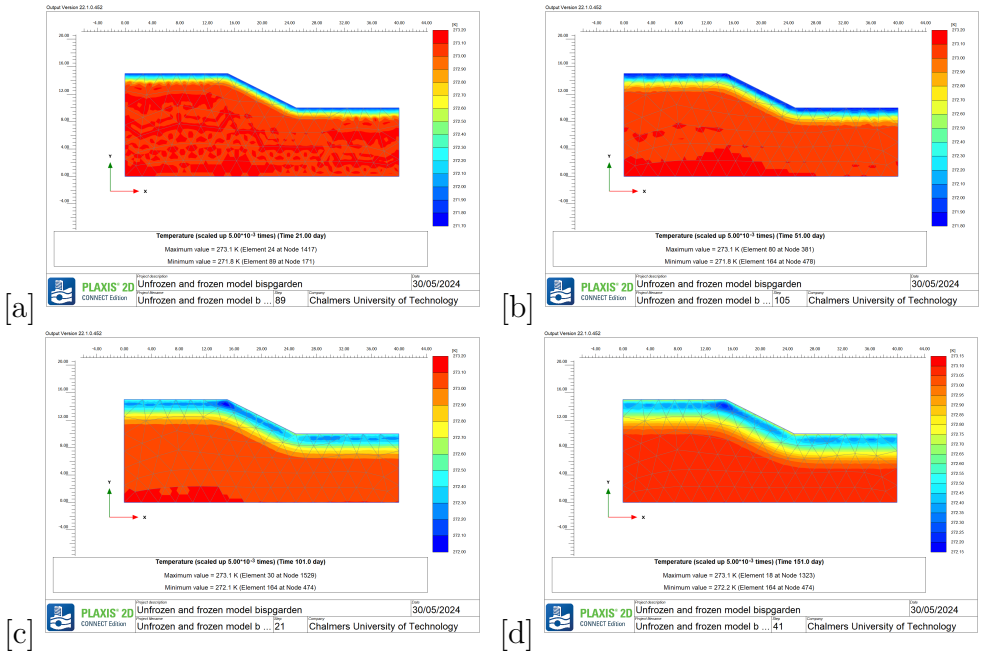

Figure 5.13: Profile of the temperature distribution when the climate is thawing and surface transfer is $1W/m^2/K$ (a) 20 days (b) 50 days (c) 100 days (d) 150 days

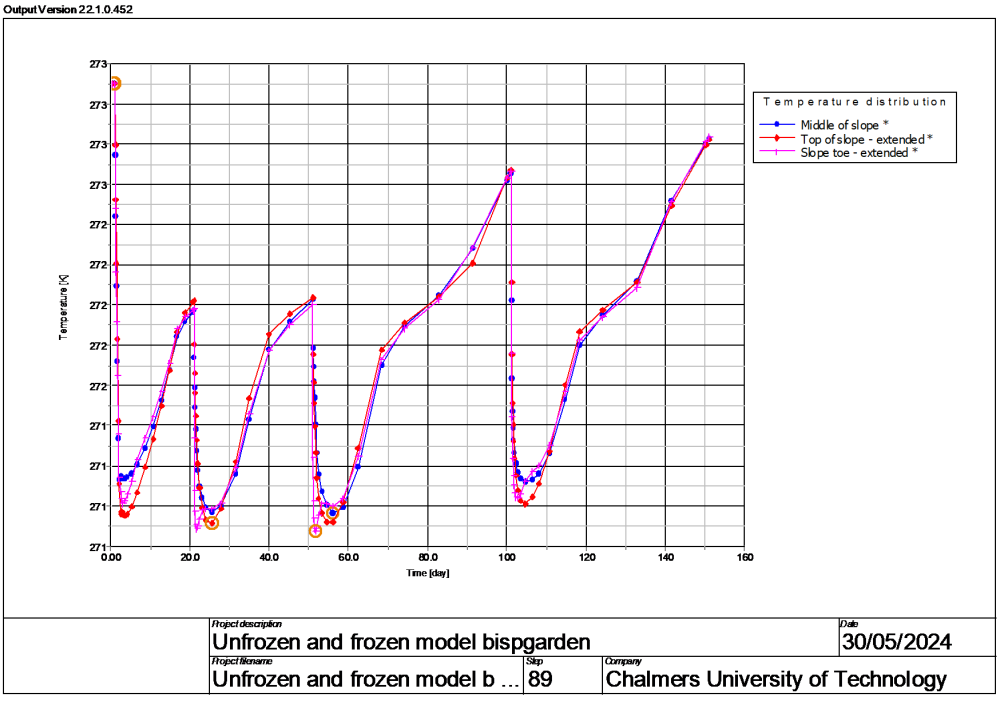

Figure 5.14: Temperature distribution when the climate is thawing and surface transfer is $1W/m^2/K$

A profile of the temperature fluctuations is illustrated in Figure 5.15. The figure shows how the climate condition boundaries affect the temperature, considering a surface transfer rate of $5W/m^2/K$ and thawing behaviour in the climate.

For the first 20 days, the maximum temperature is 273.5 K and the minimum temperature is 271.1 K. Over the next 30 days, up to day 50, the maximum temperature decreases to 273.1 K, while the minimum temperature increases to 271.4 K. During the subsequent 50 days, the maximum temperature rises to 273.3 K, and the minimum temperature rises to 271.7 K. In the final phase of the model, by day 150, the maximum temperature increases to 273.4 K, while the minimum temperature remains unchanged at 271.7 K.

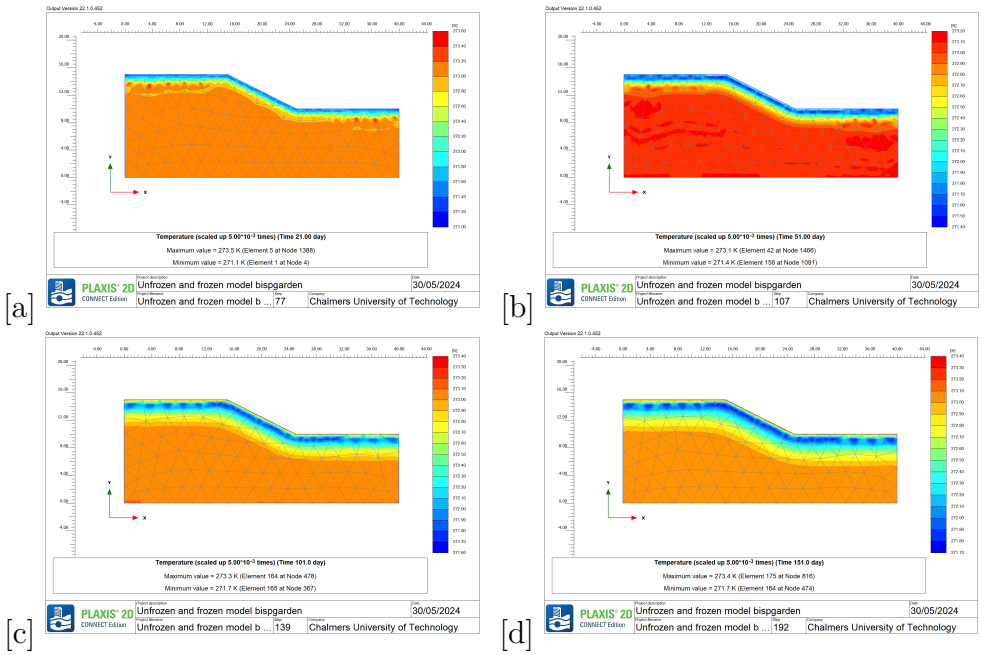

Figure 5.15: Profile of the temperature distribution when the climate is thawing and surface transfer is $5W/m^2/K$ (a) 20 days (b) 50 days (c) 100 days (d) 150 days

Figure 5.16 illustrates the temperature distribution over time with three designated nodes. The locations of these nodes are depicted in Figure 4.3. All three points exhibit similar behaviour.

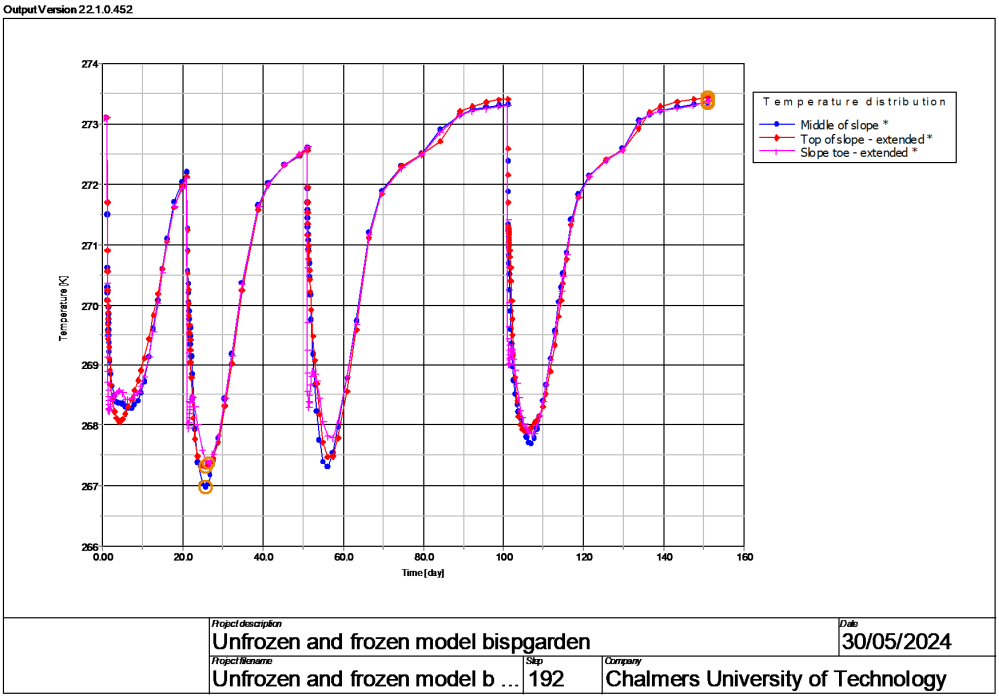

Figure 5.16: Temperature distribution when the climate is thawing and surface transfer is $5W/m^2/K$

A profile of the temperature fluctuations is illustrated in Figure 5.17. The figure shows how the climate condition boundaries affect the temperature, considering a surface transfer rate of $10W/m^2/K$ and thawing behaviour in the climate.

For the first 20 days, the maximum temperature is 273.8 K and the minimum temperature is 271.0 K. Over the next 30 days, up to day 50, the maximum temperature decreases to 273.2 K, while the minimum temperature increases to 271.3 K. During the subsequent 50 days, the maximum temperature rises to 273.7 K, and the minimum temperature rises to 271.6 K. In the final phase of the model, by day 150, the maximum temperature remains unchanged at 273.7 K, while the minimum temperature rises further to 271.7 K.

Figure 5.18 illustrates the temperature distribution over time with three designated nodes. The locations of these nodes are depicted in Figure 4.3. All three points exhibit similar behaviour.

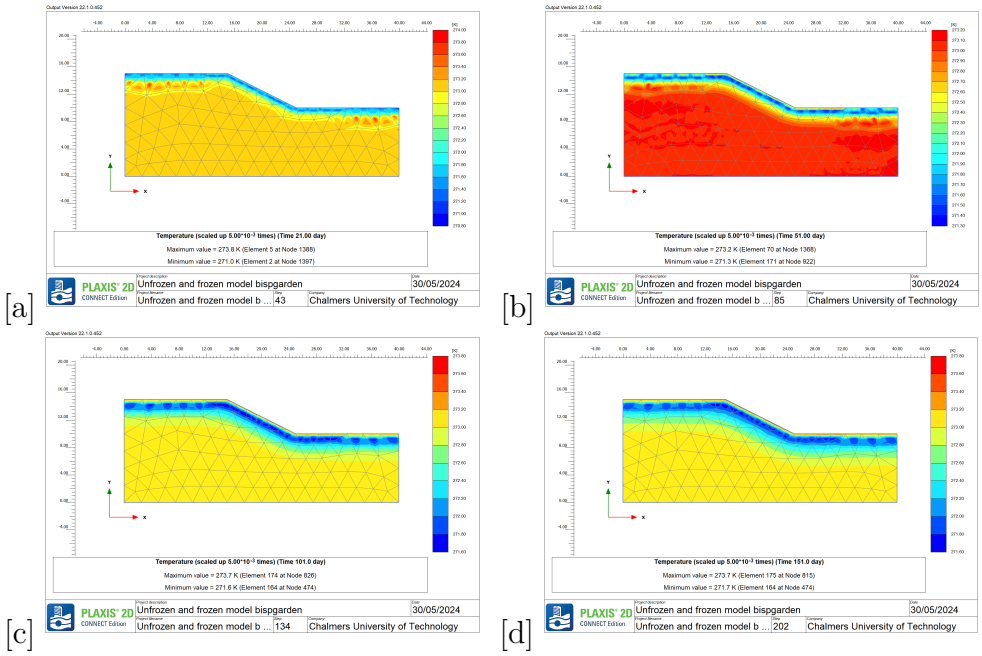

Figure 5.17: Profile of the temperature distribution when the climate is thawing and surface transfer is $10W/m^2/K$ (a) 20 days (b) 50 days (c) 100 days (d) 150 days

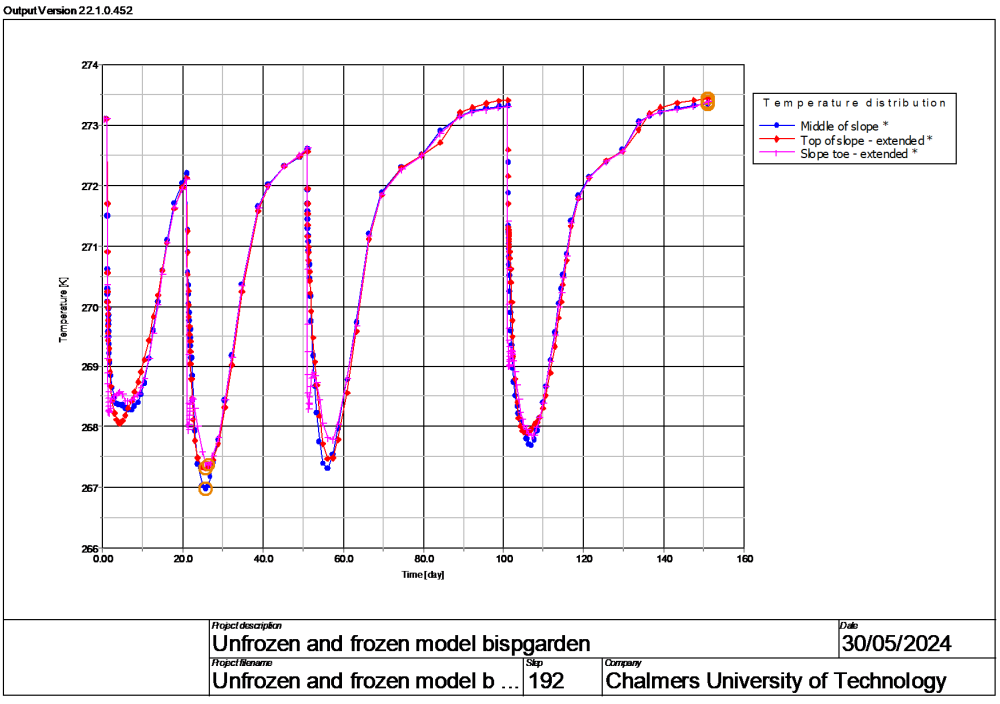

Figure 5.18: Temperature distribution when the climate is thawing and surface transfer is $5W/m^2/K$

5.2.1.2 Saturation analysis

The ice saturation in Figure 5.19 illustrates the behaviour of water over time, encompassing both freezing and thawing periods. During the thawing phase, water remains unfrozen, resulting in minimal frozen water content due to low ice saturation. The analysis reveals a maximum ice saturation of 0.1112% on the 150th day, coinciding with a surface transfer rate of $1W/m^2/K$. Conversely, during the freezing phase, water undergoes freezing, with ice saturation levels reaching as high as 49.86% on the 100th day, coinciding with a surface transfer rate of $10W/m^2/K$. See Figure 5.19

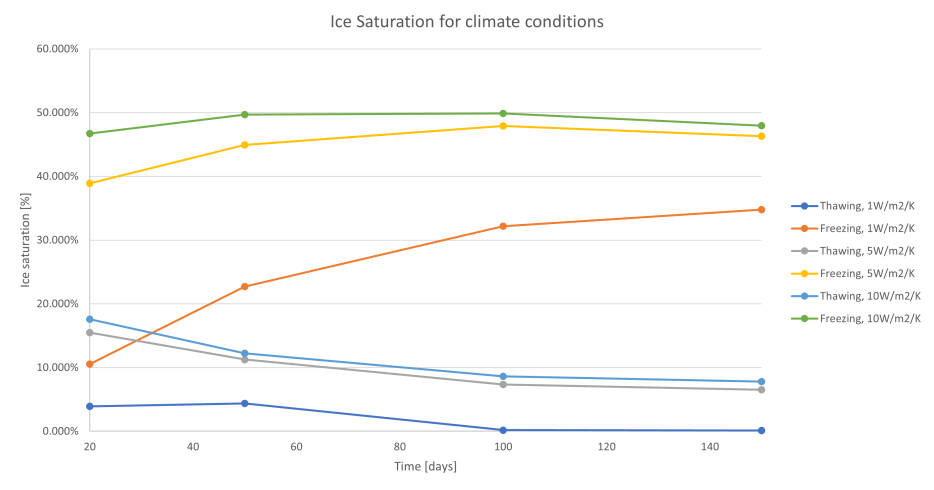

Figure 5.19: Result on how the ice saturation is distributing over time with the different climate conditions assigned

5.2.1.3 Excess pore pressure

Here are the results for the excess pore water pressure. In Plaxis, a negative value indicates compression, whereas a positive value signifies tension. Consequently, a negative pore pressure in Plaxis represents positive compressive pore water pressure.

The excess pore pressure for when the climate is freezing and has a surface transfer of $1W/m^2/K$ is shown in Figure 5.20.

During the first 20 days, the pore pressure values range from a minimum of $-0.7389\,\mathrm{kN/m^2}$ to a maximum of $-0.7852\,\mathrm{kN/m^2}$. By day 50, in the next phase, the values range from a maximum of $-2.639\,\mathrm{kN/m^2}$ to a minimum of $-2.679\,\mathrm{kN/m^2}$. In the following phase, the values range from a maximum of $-7.331\,\mathrm{kN/m^2}$ to a minimum of $-7.298\,\mathrm{kN/m^2}$. In the final phase, the values range from a maximum of $-8.310\,\mathrm{kN/m^2}$ to a minimum of $-11.16\,\mathrm{kN/m^2}$.

Overall, these results show a significant increase in compressive pore pressures over time. Initially, the pressures are low and relatively stable. As time progresses, the compressive pressures increase dramatically, indicating substantial ongoing compression. The final phase shows the highest compression levels with some variability, suggesting peak stress conditions with less uniform pressure distribution.

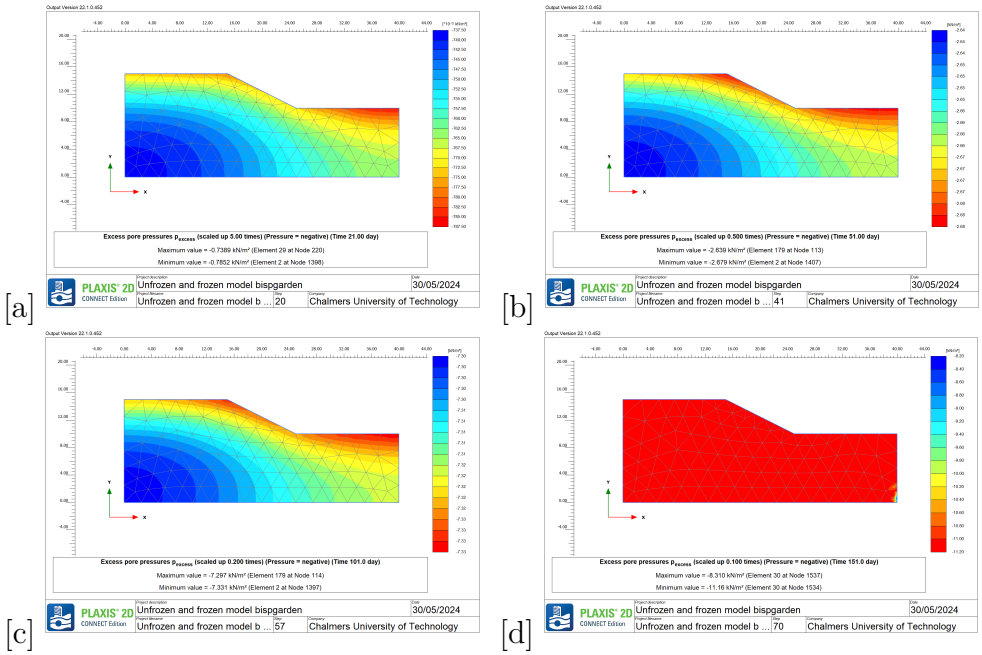

Figure 5.20: Excess pore pressure when the climate is freezing and the surface transfer is $1W/m^2/K$ for (a) 20 days (b) 50 days (c) 100 days (d) 150 days

The excess pore pressure for when the climate is freezing and has a surface transfer of $5W/m^2/K$ is shown in Figure 5.21.

During the first 20 days, the pore pressure values range from a minimum of $-4.422\,\mathrm{kN/m^2}$ to a maximum of $-4.282\,\mathrm{kN/m^2}$. By day 50, in the next phase, the values range

from a maximum of $-9.518\,\mathrm{kN/m^2}$ to a minimum of $-9.606\,\mathrm{kN/m^2}$. In the following phase, the values range from a maximum of $-6.260\,\mathrm{kN/m^2}$ to a minimum of $-6.774\,\mathrm{kN/m^2}$. In the final phase, the values range from a maximum of $-6.270\,\mathrm{kN/m^2}$ to a minimum of $-7.447\,\mathrm{kN/m^2}$.

The pore pressure undergoes fluctuations, initially showing stability, followed by significant increases and sustained compression, and ending with varied levels likely influenced by changing conditions.

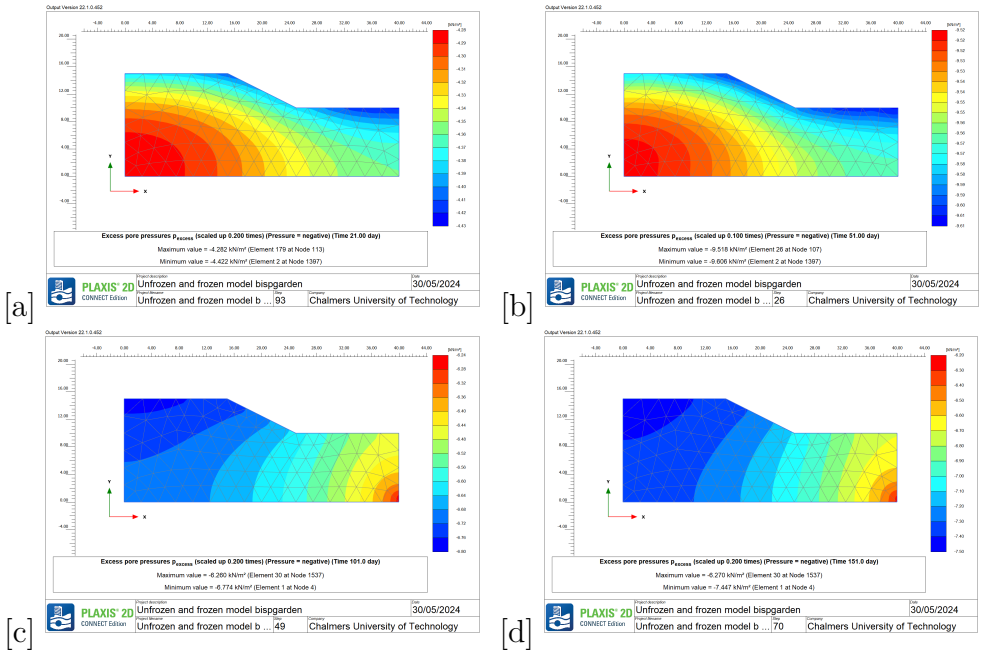

Figure 5.21: Excess pore pressure when the climate is freezing and the surface transfer is $5W/m^2/K$ for (a) 20 days (b) 50 days (c) 100 days (d) 150 days

The excess pore pressure for when the climate is freezing and has a surface transfer of $10W/m^2/K$ is shown in Figure 5.22.

During the first 20 days, the pore pressure values range from a minimum of $-6.442\,\mathrm{kN/m^2}$ to a maximum of $-6.285\,\mathrm{kN/m^2}$. By day 50, in the next phase, the values range from a maximum of $-6.278\,\mathrm{kN/m^2}$ to a minimum of $-7.763\,\mathrm{kN/m^2}$. In the following phase, the values range from a maximum of $-6.261\,\mathrm{kN/m^2}$ to a minimum of $-6.800\,\mathrm{kN/m^2}$. In the final phase, the values range from a maximum of $-6.262\,\mathrm{kN/m^2}$ to a minimum of $-6.878\,\mathrm{kN/m^2}$.

Overall, these results suggest an initial period of stable but relatively low compression, followed by a significant increase in compression by day 50. Subsequently, the compression remains relatively high but stabilizes, resulting in a narrower range of pore pressure values.

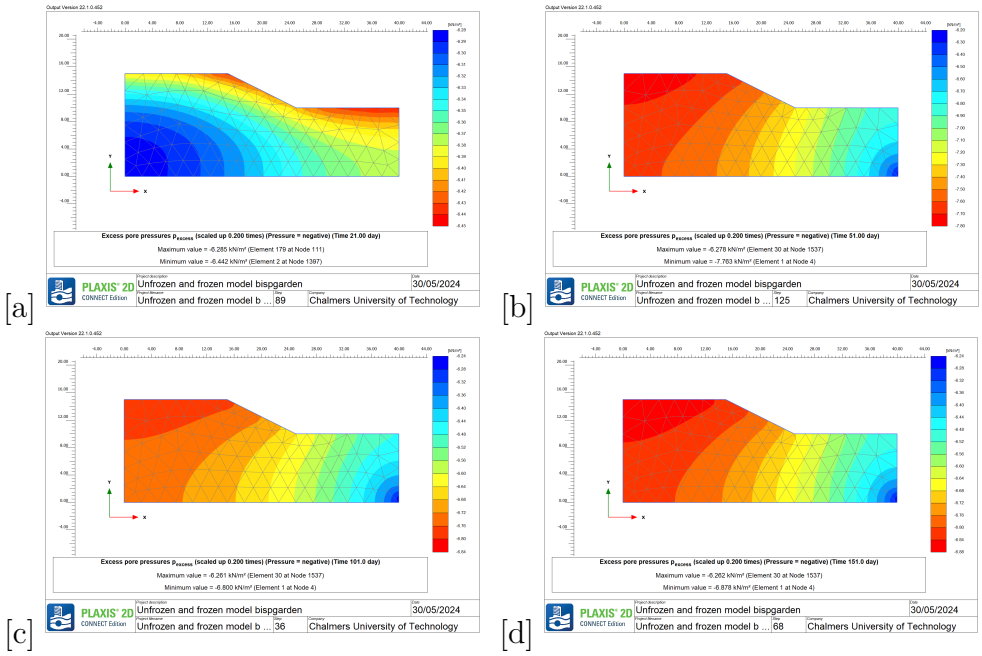

Figure 5.22: Excess pore pressure when the climate is freezing and the surface transfer is $10W/m^2/K$ for (a) 20 days (b) 50 days (c) 100 days (d) 150 days

The excess pore pressure for when the climate is thawing and has a surface transfer of $1W/m^2/K$ is shown in Figure 5.23.

During the first 20 days, the pore pressure values range from a minimum of $-0.1785\,\mathrm{kN/m^2}$ to a maximum of $-0.1528\,\mathrm{kN/m^2}$. By day 50, in the next phase, the values range from a maximum of $-0.2271\,\mathrm{kN/m^2}$ to a minimum of $-0.2489\,\mathrm{kN/m^2}$. In the following phase, the values range from a maximum of $0.2492\,\mathrm{kN/m^2}$ to a minimum of $0.2471\,\mathrm{kN/m^2}$, which suggests a transition from compression to suction. In the final phase, the values range from a maximum of $0.2912\,\mathrm{kN/m^2}$ to a minimum of $0.2907\,\mathrm{kN/m^2}$.

The narrow range of pore pressure suggests minimal fluctuation in compression within the slope. By the 100th day or phase 3, there's a transition from compression to suction, with pressures becoming more consistent. This consistently narrow range indicates stable compression, with positive pressures suggesting suction.

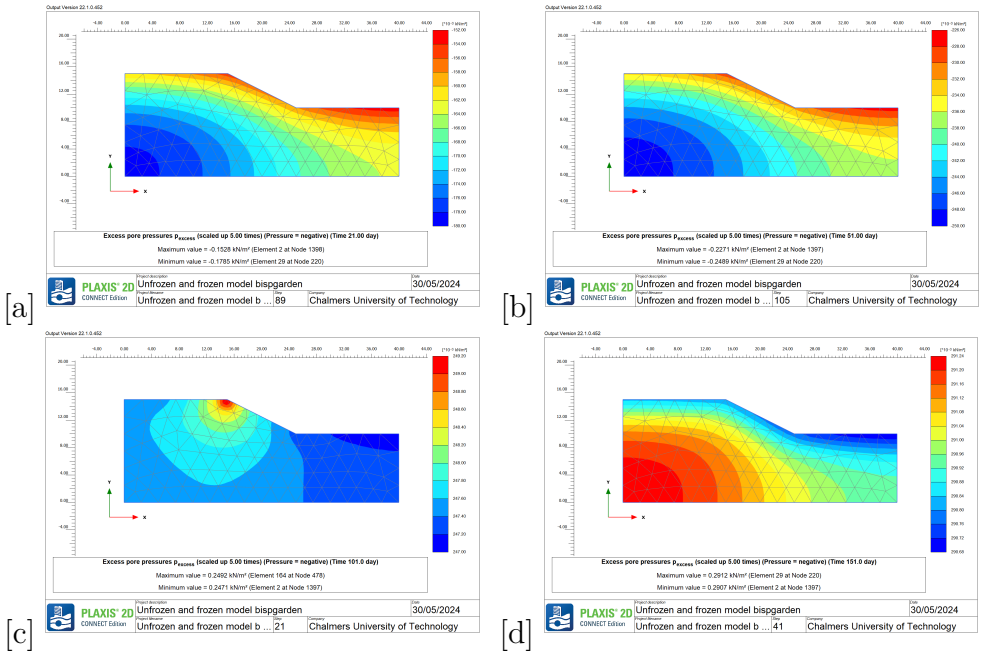

Figure 5.23: Excess pore pressure when the climate is thawing and the surface transfer is $1W/m^2/K$ for (a) 20 days (b) 50 days (c) 100 days (d) 150 days

The excess pore pressure for when the climate is thawing and has a surface transfer of $5W/m^2/K$ is shown in Figure 5.24.

During the first 20 days, the pore pressure values range from a minimum of $-3.006\,\mathrm{kN/m^2}$ to a maximum of $-2.931\,\mathrm{kN/m^2}$. By day 50, in the next phase, the values range from a maximum of $-2.473\,\mathrm{kN/m^2}$ to a minimum of $-2.533\,\mathrm{kN/m^2}$. In the following phase, the values range from a maximum of $0.1365\,\mathrm{kN/m^2}$ to a minimum of $0.1063\,\mathrm{kN/m^2}$, which suggests a transition from compression to suction. In the final phase, the values range from a maximum of $0.4408\,\mathrm{kN/m^2}$ to a minimum of $0.4175\,\mathrm{kN/m^2}$.

The pore pressure shows minimal variation, indicating stable conditions with slight compression. The narrowing range suggests further stabilization, possibly due to material settling. By the 100th day or phase 3, a transition from compression to suction occurs. The final phase exhibits a narrower range, indicating a more consistent suction effect compared to the preceding phase.

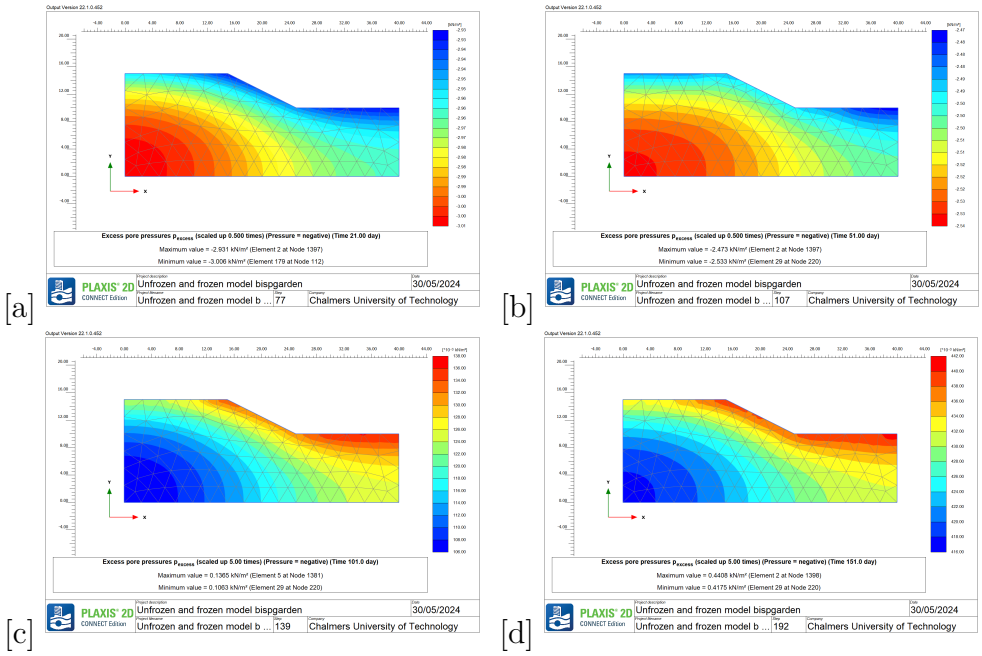

Figure 5.24: Excess pore pressure when the climate is thawing and the surface transfer is $5W/m^2/K$ for (a) 20 days (b) 50 days (c) 100 days (d) 150 days

The excess pore pressure for when the climate is thawing and has a surface transfer of $10W/m^2/K$ is shown in Figure 5.25.

During the first 20 days, the pore pressure values range from a minimum of $-3.113\,\mathrm{kN/m^2}$ to a maximum of $-3.000\,\mathrm{kN/m^2}$. By day 50, in the next phase, the values range from a maximum of $-1.010\,\mathrm{kN/m^2}$ to a minimum of $-1.071\,\mathrm{kN/m^2}$. In the following phase, the values range from a maximum of $1.606\,\mathrm{kN/m^2}$ to a minimum of $1.577\,\mathrm{kN/m^2}$, which suggests a transition from compression to suction. In the final phase, the values range from a maximum of $1.917\,\mathrm{kN/m^2}$ to a minimum of $1.890\,\mathrm{kN/m^2}$.

In the initial 20 days, a stable compression state is evident. By day 50, compression continues to narrow. Subsequently, a transition from compression to suction occurs as the range widens. Finally, a consistently narrow range suggests stable suction in the final phase.

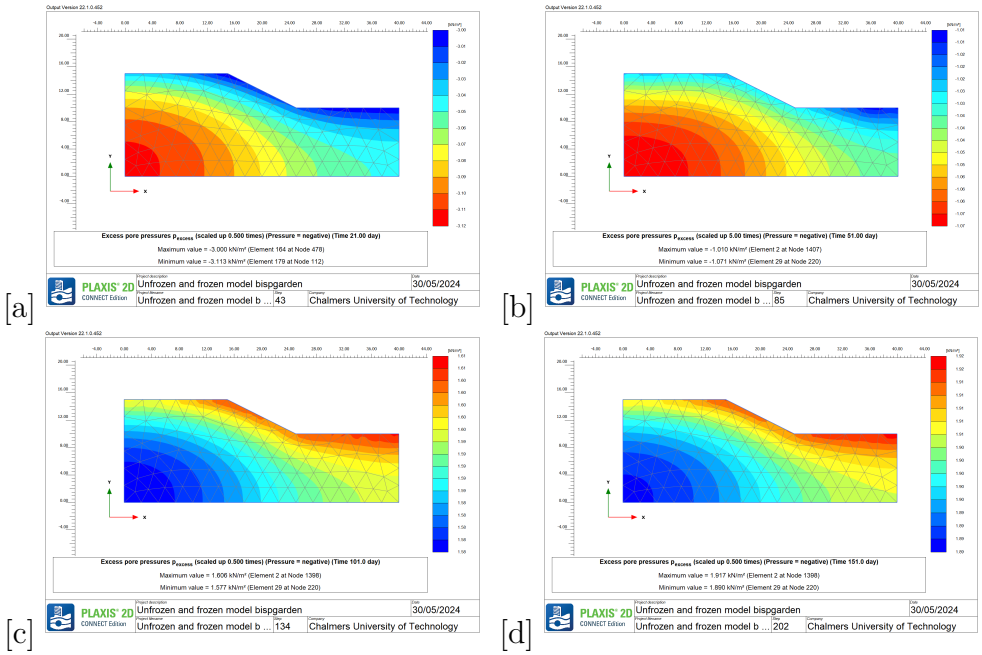

Figure 5.25: Excess pore pressure when the climate is thawing and the surface transfer is $10W/m^2/K$ for (a) 20 days (b) 50 days (c) 100 days (d) 150 days

5.2.2 Thermal flow conditions

5.2.2.1 Temperature distribution

Figure 5.26 illustrates a profile of the temperature fluctuations. The figure shows how the climate condition boundaries affect the temperature, considering thawing in the soil's thermal flow, so the temperature in the soil is increasing.

During the initial 20 days, the maximum temperature reaches 293.1 K, while the minimum temperature is 273.0 K. Over the following 30 days, up to day 50, the maximum temperature rises to 293.4 K, and the minimum temperature increases to 271.3 K. Subsequently, during the next 50 days, the maximum temperature decreases to 293.3 K, while the minimum temperature increases to 273.1 K. In the final phase of the model, by day 150, the maximum temperature (293.3 K) and the minimum temperature (273.1 K) remain unchanged from the previous phase.

Figure 5.27 shows how the temperature fluctuates with different selected points shown in Figure 4.3. The midpoint of the slope initially exhibits shallow fluctuations in the first few days. From around day 5, there is a rapid increase until day 40, followed by a slight stabilization but continued gradual increase until day 150. On the other hand, the slope toe point shows greater fluctuations initially, then experiences a more rapid increase until around day 18 or just under 20 days. Afterwards, there is no significant change until day 150.

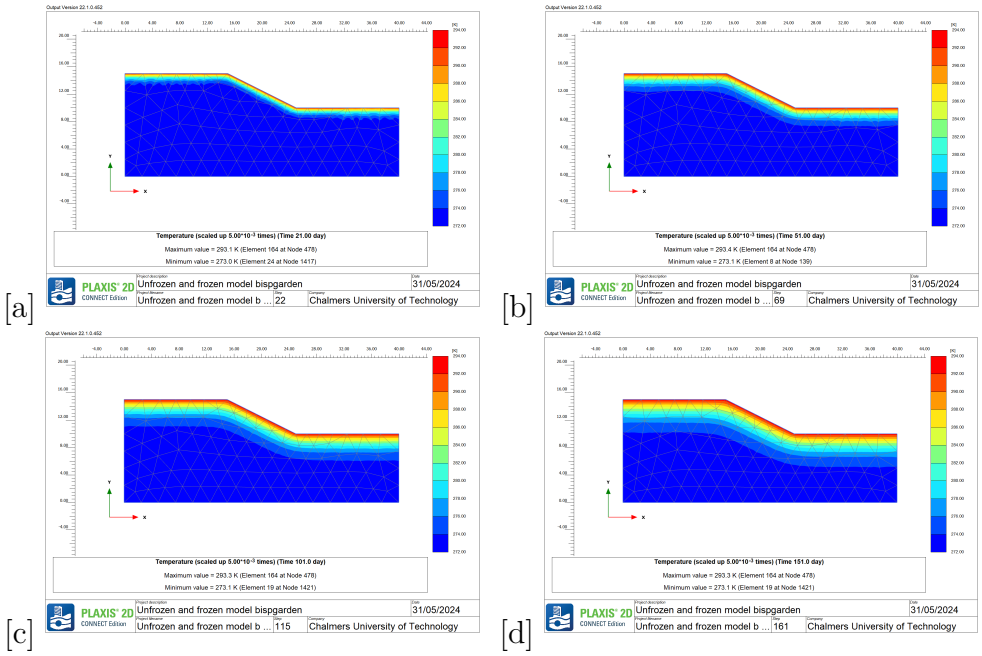

Figure 5.26: Profile of the temperature distribution when the thermal flow is thawing in the soil for (a) 20 days (b) 50 days (c) 100 days (d) 150 days

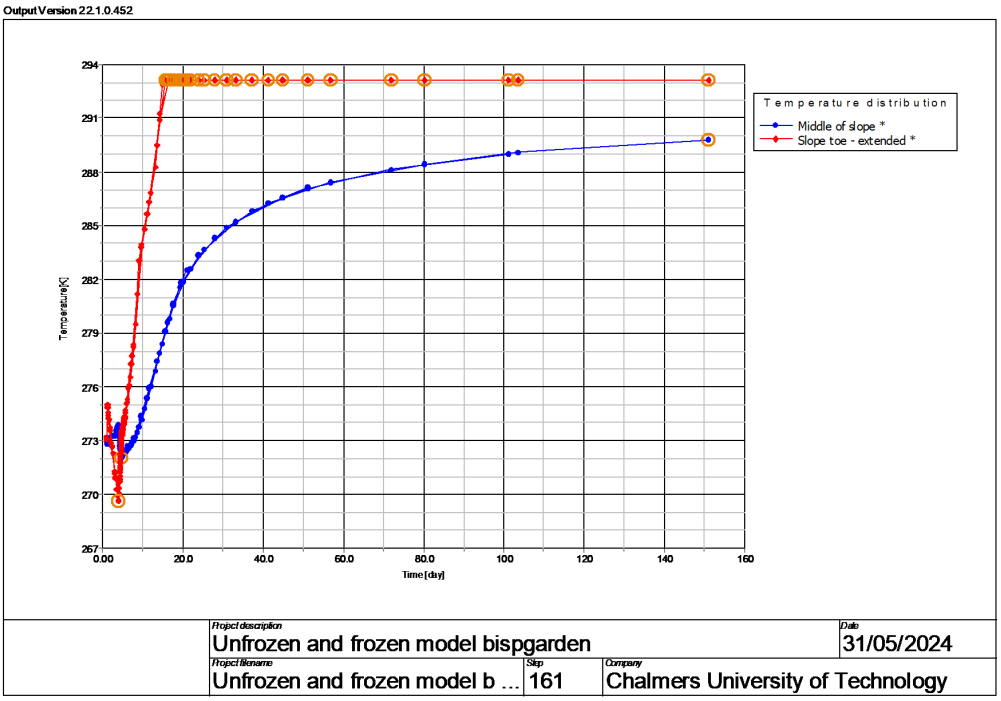

Figure 5.27: Temperature distribution when thermal flow is thawing.

Figure 5.28 illustrates a profile of the temperature fluctuations. The figure shows how the climate condition boundaries affect the temperature, considering freezing in the soil's thermal flow, so the temperature in the soil is decreasing.

During the initial 20 days, the maximum temperature reaches 274.4 K, while the minimum temperature is 251.5 K. Over the following 30 days, up to day 50, the maximum temperature decreases to 273.6 K, and the minimum temperature decreases to 250.8 K. Subsequently, during the next 50 days, the maximum temperature decreases further to 273.2 K, while the minimum temperature increases to 250.9 K. In the final phase of the model, by day 150, the maximum temperature decreases further to 273.1 K and the minimum temperature increases again 251.0 K.

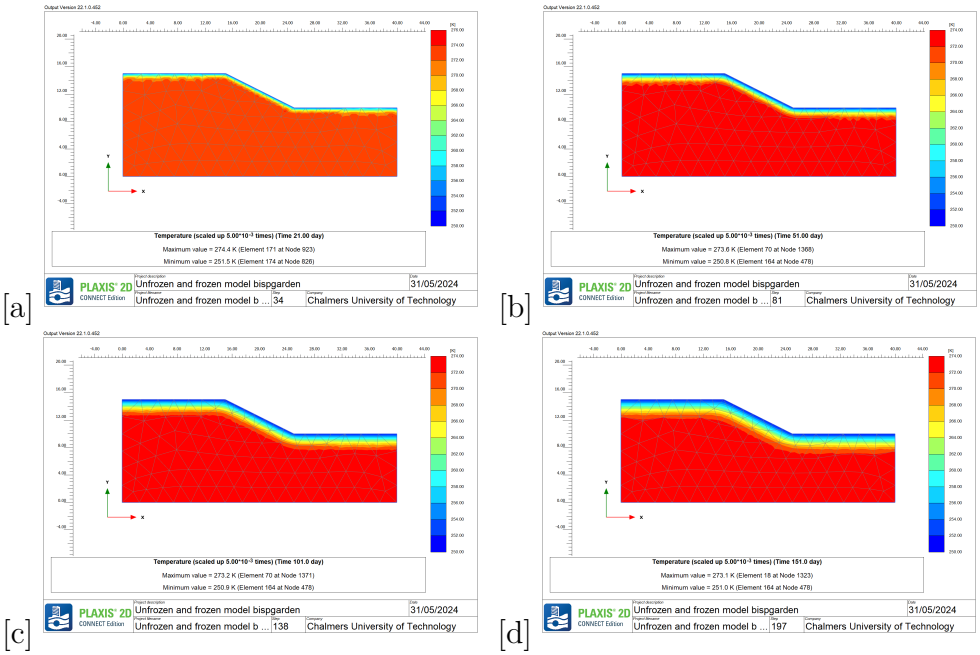

Figure 5.28: Profile of the temperature distribution when the thermal flow is freezing in the soil for (a) 20 days (b) 50 days (c) 100 days (d) 150 days

Figure 5.29 shows how the temperature fluctuates with different selected points shown in Figure 4.3. Initially, the midpoint of the slope shows slight fluctuations in the first few days. Starting from around day 5, there is a rapid decrease until day 40, followed by a slight stabilization but continued gradual decrease until day 150. Conversely, the slope toe point initially increases, then experiences a more rapid decrease until around day 20. Thereafter, there is no significant change until day 150.

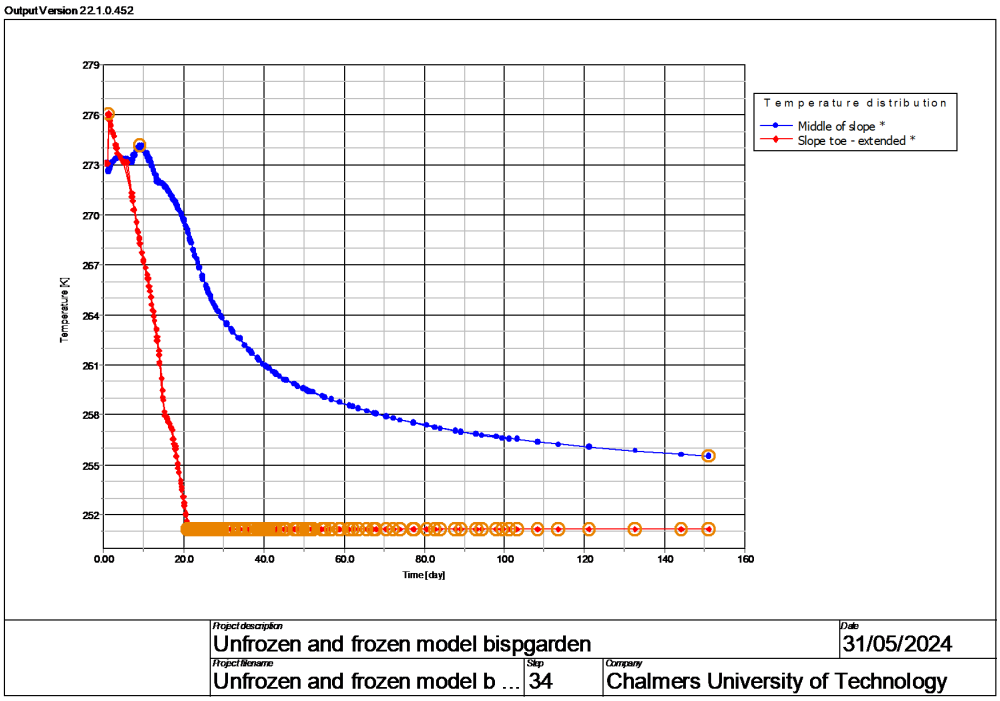

Figure 5.29: Temperature distribution when the thermal flow is freezing.

5.2.2.2 Saturation analysis

Figure 5.30 is a diagram of how the ice saturation behaves in the soil when the thermal flow is freezing.

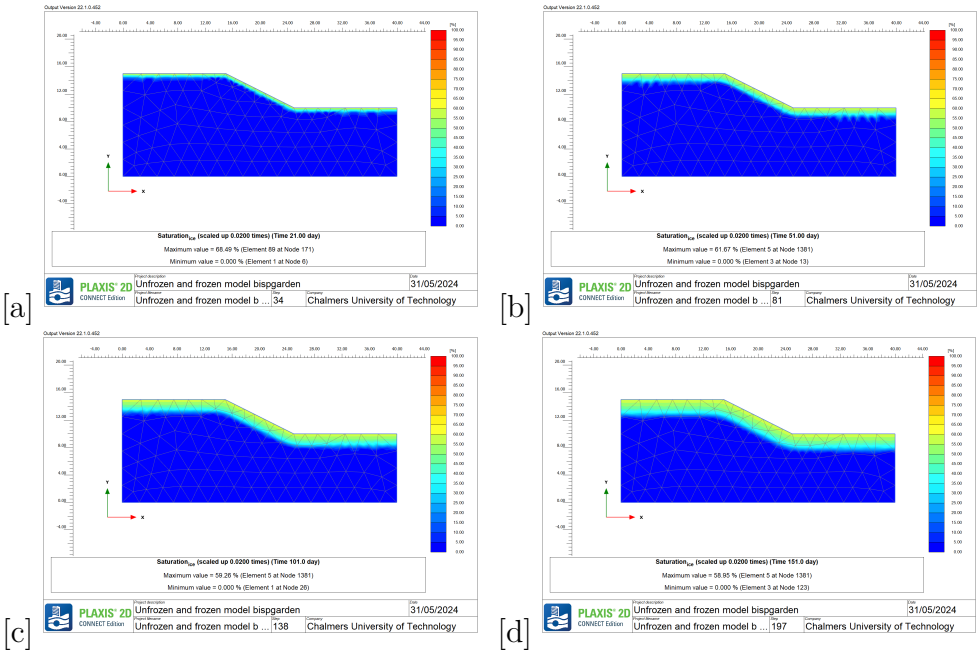

Figure 5.30: Profile of the ice saturation when the thermal flow is freezing in the soil for (a) 20 days (b) 50 days (c) 100 days (d) 150 days

Figure 5.31 shows the ice saturation in the soil distributed on days when the soil is freezing. It reveals a peak ice content on day 20, followed by a gradual decrease over time. However, the ice saturation does not drop below 58% throughout the observed period.

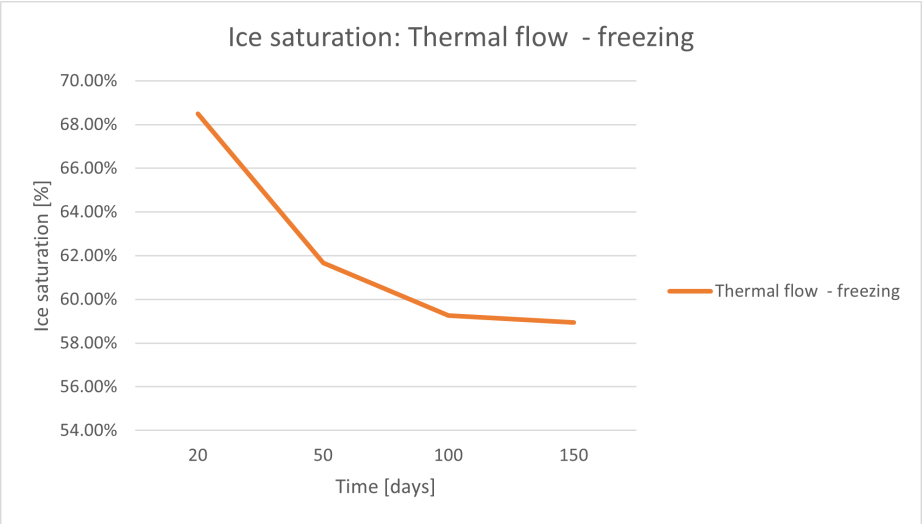

Figure 5.31: Ice saturation when boundary conditions are thermal flow is freezing.

Figure 5.32 is a diagram of how the ice saturation is behaving in the soil when the thermal flow is thawing.

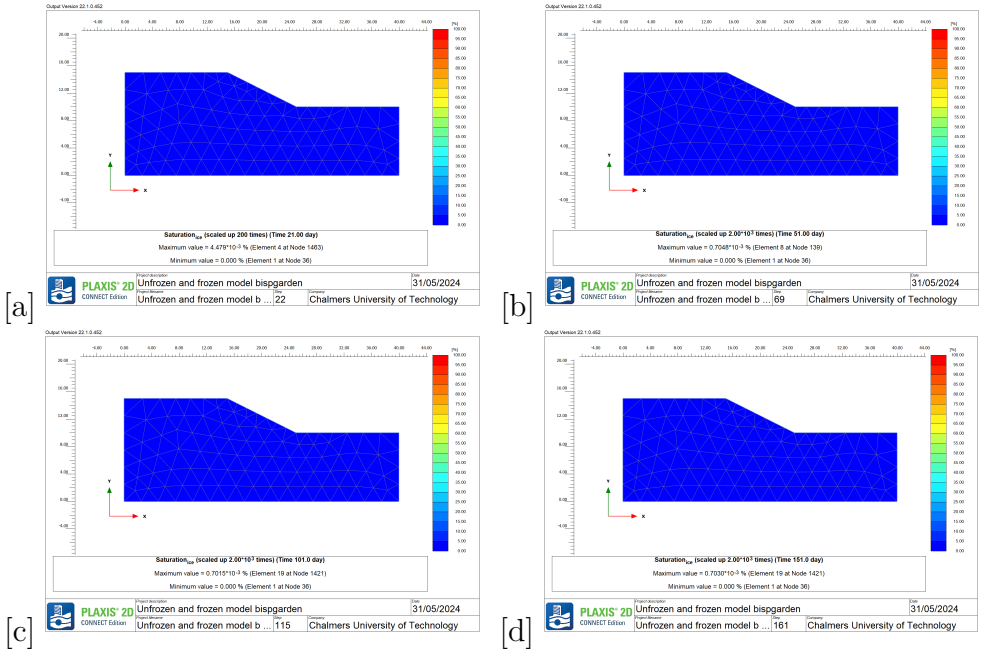

Figure 5.32: Profile of the ice saturation when the thermal flow is thawing in the soil for (a) 20 days (b) 50 days (c) 100 days (d) 150 days

Figure 5.33 shows the ice saturation in the soil distributed on days when the soil is thawing. The results show almost no ice in the soil when the thermal flow conditions are thawing. Additionally, it does not change between days 50 to 150.

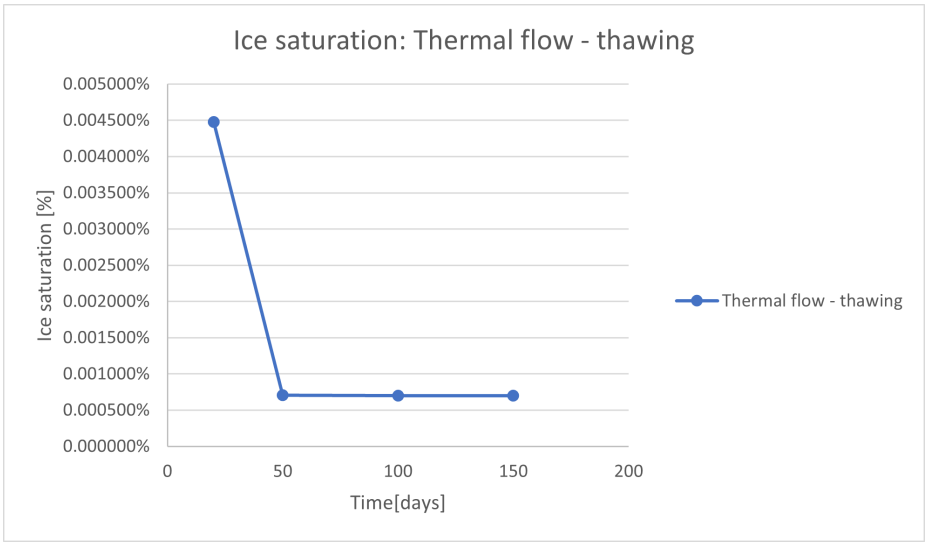

Figure 5.33: Ice saturation when boundary conditions are thermal flow is thawing.

5.2.2.3 Excess pore pressure

The excess pore pressures under thawing thermal flow conditions are illustrated in Figure 5.34.

During the first 20 days, the pore pressure values range from a minimum of $-0.7852\,\mathrm{kN/m^2}$ to a maximum of $-0.7389\,\mathrm{kN/m^2}$. By day 50, in the next phase, the values range from a maximum of $-2.639\,\mathrm{kN/m^2}$ to a minimum of $-2.679\,\mathrm{kN/m^2}$. In the following phase, the values range from a maximum of $-5.531\,\mathrm{kN/m^2}$ to a minimum of $-5.539\,\mathrm{kN/m^2}$. In the final phase, the values range from a maximum of $-6.915\,\mathrm{kN/m^2}$ to a minimum of $-6.920\,\mathrm{kN/m^2}$.

Overall, these results show that the compressive pore water pressures increase substantially over time. Initially, there is more variation in the pressures, but as time progresses, the pressures not only increase but also become more uniform. This suggests that the material or system is undergoing significant compression, which stabilizes over time, leading to less variation in the measured pressures.

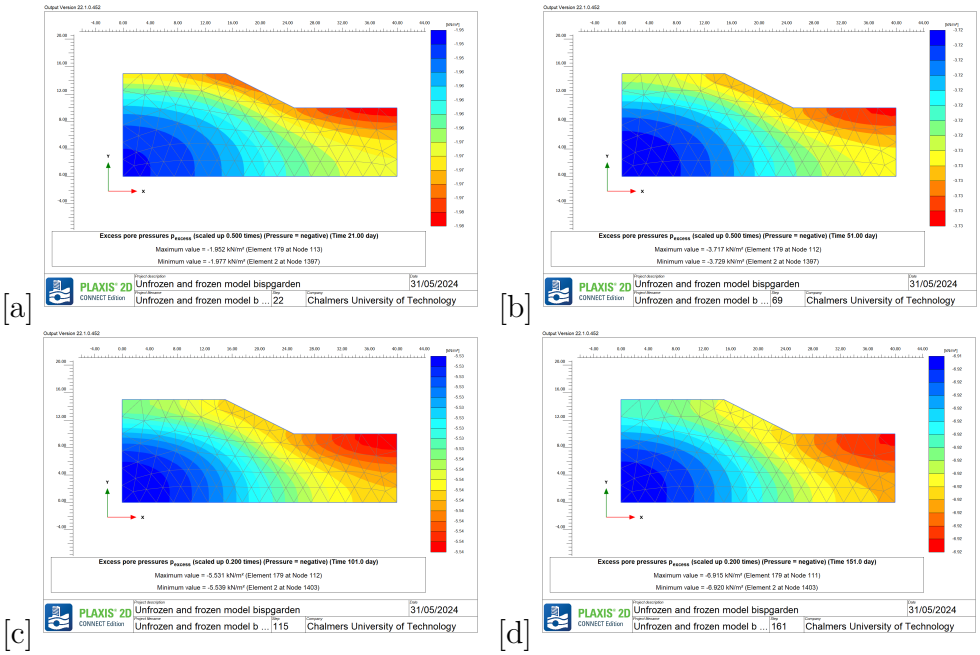

Figure 5.34: Profile of the excess pore pressure when the thermal flow is thawing in the soil for (a) 20 days (b) 50 days (c) 100 days (d) 150 days

The excess pore pressures under freezing thermal flow conditions are shown in Figure 5.35.

During the first 20 days, the pore pressure values range from a minimum of $-8.929\,\mathrm{kN/m^2}$ to a maximum of $-6.303\,\mathrm{kN/m^2}$. By day 50, in the next phase, the values range from a maximum of $-6.270\,\mathrm{kN/m^2}$ to a minimum of $-7.298\,\mathrm{kN/m^2}$. In the subsequent phase, the values range from a maximum of $-6.264\,\mathrm{kN/m^2}$ to a minimum of $-6.953\,\mathrm{kN/m^2}$. In the final phase, the values range from a maximum of $-6.260\,\mathrm{kN/m^2}$ to a minimum of $-6.803\,\mathrm{kN/m^2}$.

These results indicate that over time, the range of pore pressure values narrows and the overall compressive pore water pressure decreases. Initially, there is a wider variation in pore pressure, with a high level of compression. As time progresses, the maximum pore pressure values decrease, showing less variation and indicating that the compressive forces are becoming more uniform. This trend suggests that the material is undergoing significant compression, stabilizing over time with reduced pressure variations.

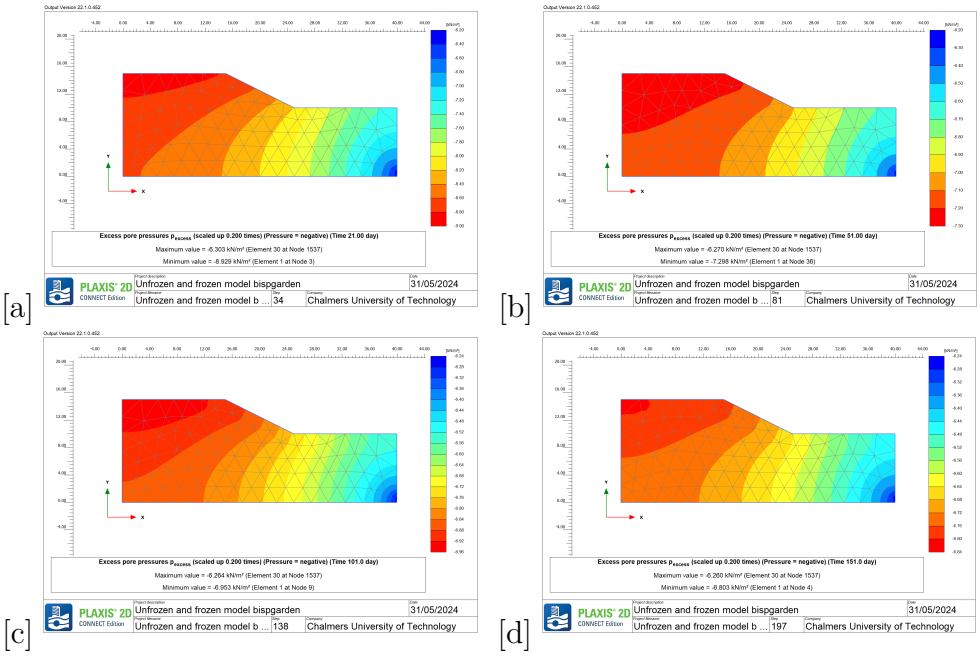

Figure 5.35: Profile of the excess pore pressure when the thermal flow is freezing in the soil for (a) 20 days (b) 50 days (c) 100 days (d) 150 days

5.3 Safety Factor analysis

5.3.1 BC: Climate in Jämtland

From Figure 5.36 the SF is experiencing some variation along the time period. As can also be seen from this figure, when the climate is freezing the safety factor of the slope is lowered with time. Additionally, when climate is experiencing thawing the safety factor increases with time. It looks also like the slope safety factor is less dependent on heat changes and surface transfer during the thawing period and on the other hand the safety factor drops more with time during the freezing period and drops faster with time with higher surface transfer. See Tables C.1 and C.2 for full results.

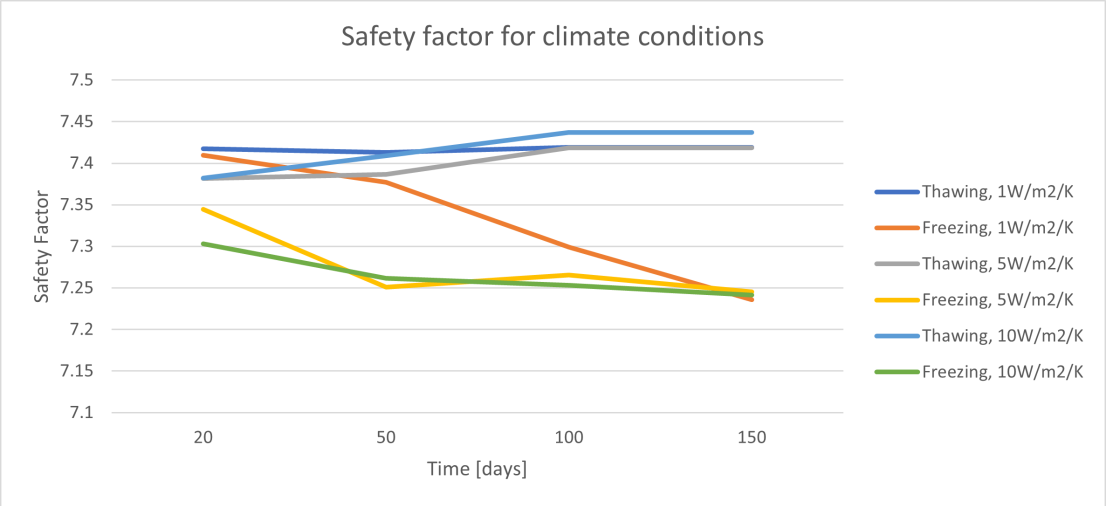

Figure 5.36: A distribution on how the SF is acting with different climate conditions from hand calculations

From Figure 5.37 the safety factor remains steady throughout the analysis, showing no fluctuations. The figure also indicates that when the surface transfer is$1W/m^2/K$ the freezing and thawing climates cause minimal change. However, a more significant difference is observed between the other two surface transfer rates analyzed, depending on whether the conditions are freezing or thawing.

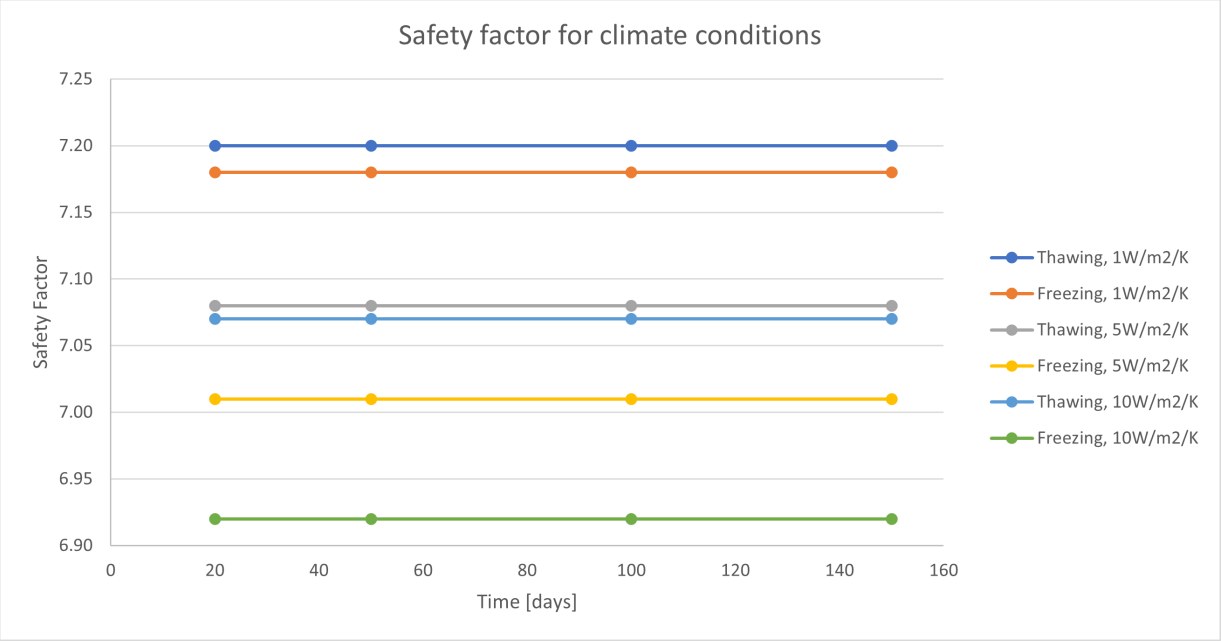

Figure 5.37: A distribution on how the SF is acting with different climate conditions from python code

Figure 5.38 illustrates the ice saturation under specific climate conditions, with a surface transfer rate of $10\text{W/m}^2\text{K}$ after 150 days of freezing. The results show a safety factor (SF) of 6.92, a radius (R) of 13 meters, and a critical point located at $X_c, Y_c = (20.40, 21.20)$. As depicted in Figure 5.38, the depth of the slip surface and the extent of ice saturation after 150 days occupy only a small portion of the slip surface and do not significantly impact it.

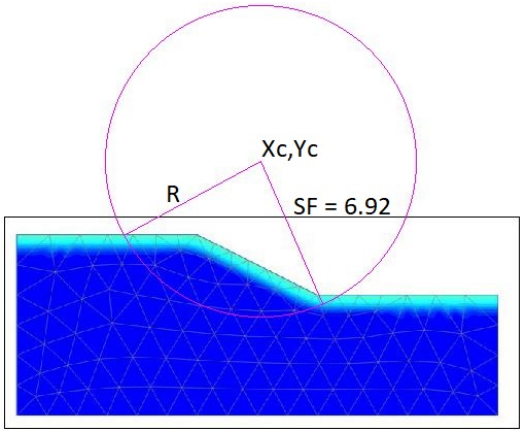

Figure 5.38: A diagram illustrating the slip surface under climate conditions, with a surface transfer rate of $10w/m^2/k$ after 150 days of freezing temperature

5.3.2 BC: Thermal flow

From Figure 5.39 the safety factor appears steady and without any fluctuations. The main difference is observed when comparing the two calculation methods: the hand calculations yield a lower outcome, while the Python tool produces a higher outcome. See Tables C.3 and C.4 for full results.

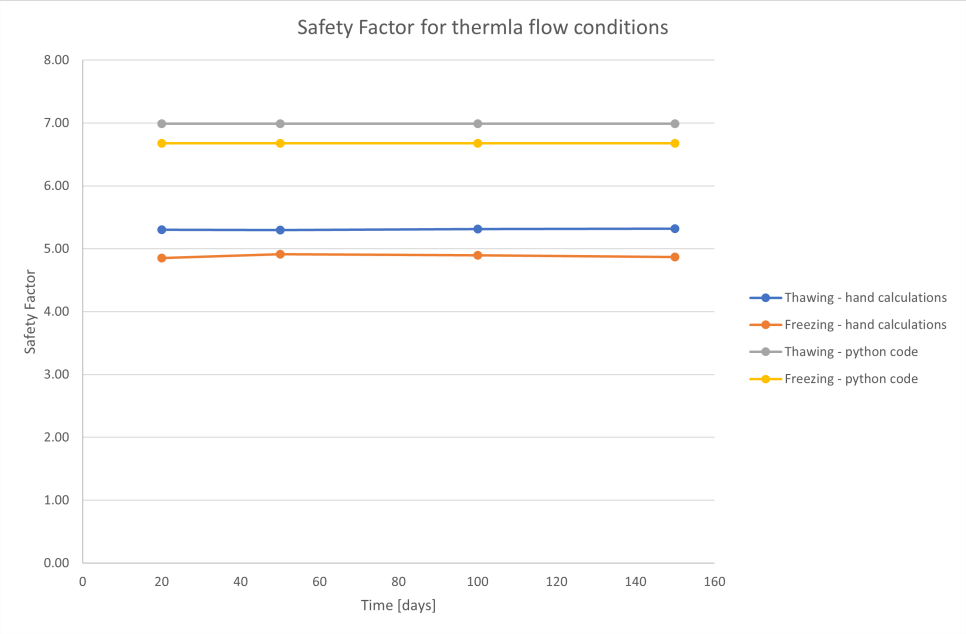

Figure 5.39: A distribution on how the SF is acting with different climate conditions from hand calculations and python code

Figure 5.40 shows a diagram of ice saturation under thermal flow freezing conditions over 150 days. The results indicate a safety factor (SF) of 6.68, a radius (R) of 13 meters, and a critical point at coordinates $X_c, Y_c = (20.40, 21.20)$. As illustrated, the depth of the slip surface and the extent of ice saturation after 150 days occupy a slightly larger portion of the slip surface compared to Figure 5.38, yet still have no significant impact on slope stability.

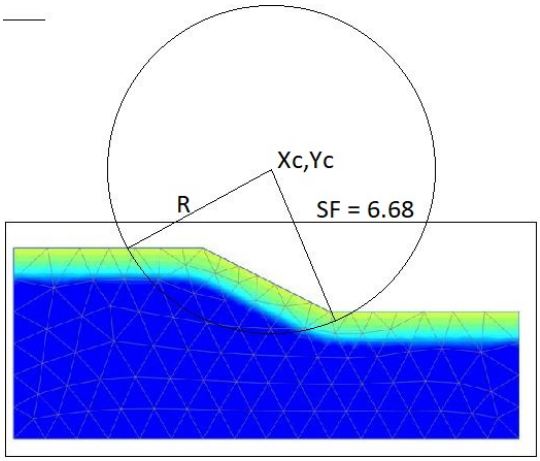

Figure 5.40: A diagram illustrating the slip surface under thermal flow conditions after 150 days of freezing temperature

6

Discussion

The FU model employs two sets of boundary conditions: one based on climate data from the Jämtland region and another based on assigned thermal flow in the soil. The temperature functions simulate seasonal transitions, specifically thawing (frozen soil to thawed soil) and freezing (thawed soil to frozen soil).

6.1 Thermal influence

The model evaluates temperature distribution over a period of 150 days. Different scenarios are analyzed, including summer-to-autumn and winter-to-spring transitions, with various surface transfer rates ($1W/m^2/K, 5W/m^2/K, and 10W/m^2/K$). This allows for understanding how thermal energy moves through the soil and affects its thermal profile. It also uses an assigned thermal flow temperature function. The results show a larger range in temperature with a larger surface transfer rate. Also, the thermal flow temperature functions show a large variation in days with freezing and thawing in the soil.

Soil thermal conductivity, which denotes the soil's ability to conduct heat, is influenced by factors such as soil type and porosity. Soils with higher thermal conductivity can efficiently transfer heat, resulting in faster temperature variations within the soil mass. Notably, the soil thermal conductivity remained consistent throughout the analysis, potentially impacting the results under both the boundary conditions of climate in the area and thermal flow.

6.2 Saturation analysis

The results of the saturation analysis are consistent with expected seasonal patterns, where warmer temperatures prevent extensive ice formation within the soil. Moreover, soil transition from a liquid to a solid phase during freezing can alter its moisture content and potentially lead to frost heave, a phenomenon where the expansion of frozen soil can cause ground upheaval.

As seen from the results the ice saturation varies with seasonal changes. During colder periods, the freezing of the soil increases ice saturation, peaking early in the freeze period and then gradually decreasing as the freezing progresses.

Increased ice saturation affects the slope stability by altering the soil's mechanical properties. The safety factor of the slope decreases during freezing conditions due to higher ice saturation.

6.3 Excess pore pressure

Excess pore pressure in freezing soils is influenced by cryogenic suction, which is the pressure difference between the ice and unfrozen water in the soil. As the soil freezes, cryogenic suction increases, leading to higher excess pore pressure also leading to changes in the effective stresses.

During freezing, the formation of ice lenses can expel water from the pores, increasing excess pore pressure. Conversely, during thawing, the melting of ice can release this pressure suddenly, potentially leading to soil instability and an increased risk of landslides or other failures.

6.4 Safety factor

The consistent safety factor (SF) values observed in the results suggest that the slope exhibits stable behaviour under the analyzed conditions. This consistency implies resilience to changes in influencing factors, indicating a robust performance against potential failure mechanisms. In this analysis, variations in SF during freezing and thawing conditions are primarily influenced by soil properties and thermal effects.

In freezing conditions, the formation of ice lenses within the soil matrix can elevate pore pressure and diminish shear strength. Conversely, during thawing, the soil often gains strength as ice melts and pore water redistributes, fostering enhanced soil-to-soil contact and particle interlocking. Thermal expansion and contraction of soil particles and pore water throughout freezing and thawing cycles can generate internal stresses within the soil mass, potentially resulting in soil cracking, structural disruption, and alterations in pore pressure distribution, all of which impact soil stability. However, the analysis results suggest that none of these mechanisms occurred in this particular study.

The minimal change observed in the safety factor results in a $1W/m^2/K$ surface transfer rate indicating a slower rate of heat transfer, resulting in gradual temperature fluctuations within the soil mass. Conversely, higher surface transfer rates may prompt quicker temperature changes, leading to increased thermal stresses and fluctuations in soil properties over time.

Based on the analysis, it appears that these boundary conditions do not require significant mitigation measures to address freezing and thawing cycles.

7
Conclusion

The findings of this study highlight several key aspects regarding the impact of freeze-thaw cycles on slope stability:

- The rate of the surface transfer seems to be sensitive in the scenario of when the boundaries were set as climate conditions.
- Low ice saturation indicates that the soil remains in a predominantly unfrozen state, which affects its thermal conductivity and hydraulic properties.
- The Safety factor is lower when the thermal flow boundaries are used. The slope appears to be more stable.

7.1 Limitations

A model serves as a simplified depiction of intricate systems or phenomena, aiding in the comprehension, analysis, and decision-making processes concerning real-world scenarios. By dissecting complex situations into more digestible components, models facilitate understanding and enable effective problem-solving [20].

There has been throughout the report mentioned on limitations both with the FU model and the collected parameters and inputs for the FU model. As an example, the temperature functions and the time set for the analysis do not seem to go deep enough so it is affecting the slip surface.

7.2 Further studies

The study does not include precipitation but it is mentioned in the Introduction that there has been an increase in precipitation in the past decade. It is recommended to include precipitation data in the model from the area for a more realistic analysis.

Look at other climate data, maybe older data and compare it with a new climate data set in the area. This would show if there is in fact how the temperature is developing in the area and how it is affecting the stabilisation on the slope.

The surface transfer rates that were assigned showed changes and could include other surface rates in the analysis. Also, the length of the analysis could have been longer.

Additionally, perform a sensitivity analysis to determine which parameters most significantly impact the safety factor in both freezing and thawing conditions.

It is recommended to monitor the slope stability under varying climatic conditions and longer time.

By addressing these limitations and conducting further studies, future research can enhance our understanding of slope stability in regions affected by freeze-thaw cycles and contribute to the development of more robust engineering solutions.

Bibliography

[1] Bračko, T., Žlender, B., and Jelušič, P,. (2022) *Implementation of Climate Change Effects on Slope Stability Analysis*. Applied Sciences, 12(16), 8171. https://doi.org/10.3390/app12168171.

[2] Kandalai, S., John, N. J., and Patel, A. (2023). Effects of climate change on geotechnical infrastructures—state of the art. Environmental Science and Pollution Research, 30(7), 16878-16904. https://doi.org/10.1007/s11356-022-24788-7.

[3] P. Koorevaar, G. Menelik, C. Dirksen, (1983). 7 Heat Transport in Soil Developments in Soil Science. Elsevier. Volume 13. 193-207. https://doi.org/10.1016/S0166-2481(08)70054-0.

[4] Lantmäteriet. (n.d.). Min Karta. https://minkarta.lantmateriet.se/

[5] Lundström, K., & Andersson, M. (2008). Växter som skydd mot erosion och ytliga ras i branta jordslänter Demonstrationsförsök i Bispgården och Bydalen (tech. rep.)

[6] FREMOND, D BLANCHARD M., (1982) CRYOGENIC SUCTION IN SOILS, I IIIIIIEImI EIIIIIIEIIEIIE, 22, 233.

[7] Nylén, L., Asp, M., Berggreen-Clausen, S., Berglöv, G., Björck, E., Axén Mårtensson, J., Ohlsson, A., Persson, H., & Sjökvist, E. (2015). Framtidsklimat i Jämtlands län - enligt RCP-scenarier. KLIMATOLOGI, (34).

[8] Nishimura, S., Gens, A., Olivella, S., & Jardine, R. J. (2009). THM-coupled finite element analysis of frozen soil: formulation and application. Géotechnique, 59(3), 159-171.

[9] Andersland, O. B., & Ladanyi, B. (2003). Frozen ground engineering. John Wiley & Sons.

[10] Thomas, H. R., Cleall, P., Li, Y. C., Harris, C., & Kern-Luetschg, M. (2009). Modelling of cryogenic processes in permafrost and seasonally frozen soils. Geotechnique, 59(3), 173-184.

[11] Taber, S. (1929). Frost heaving. The Journal of Geology, 37(5), 428-461.

[12] Geological Survey of Sweden. (n.d.). SGU Map viewer. https://www.sgu.se/en/products/maps/map-viewer/

[13] Krahn, J. (2003). The 2001 RM Hardy Lecture: The limits of limit equilibrium analyses. Canadian geotechnical journal, 40(3), 643-660.

[14] Karstunen, M., & Amavasai, A. (2017). BEST SOIL: Soft soil modelling and parameter determination.

[15] IPCC (2007) Climate change: Climate change impacts, adaptation, and vulnerability. In: Working Group II contribution to Intergovernmental panel on climate change Fourth Assessment Report. Summary for policymakers

[16] Salunkhe, D. P., Bartakke, R. N., Chvan, G., Kothavale, P. R., & Digvijay, P. (2017). An overview on methods for slope stability analysis. International Journal of Engineering Research & Technology (IJERT), 6(03), 2278-0181.

[17] Ghoreishian Amiri, S.A., Grimstad, G., Aukenthaler, M., Panagoulias, S., Brinkgreve, R.B.J., Haxaire, A. (2016a). The Frozen and Unfrozen Soil Model Manual.

[18] Ghoreishian Amiri, S. A., Grimstad, G., Kadivar, M., & Nordal, S. (2016b). Constitutive model for rate-independent behavior of saturated frozen soils. Canadian Geotechnical Journal, 53(10), 1646-1657.

[19] Zhang, X., Alonso, E. E., & Casini, F. (2016). Explicit formulation of at-rest coefficient and its role in calibrating elasto-plastic models for unsaturated soils. Computers and Geotechnics, 71, 56-68.

[20] Wood, D. M. (2017). Geotechnical modelling. CRC press.

[21] Vardon, P. J. (2015). Climatic influence on geotechnical infrastructure: a review. Environmental Geotechnics, 2(3), 166-174.

[22] Subramanian, S. S., Ishikawa, T., & Tokoro, T. (2017). Stability assessment approach for soil slopes in seasonal cold regions. Engineering geology, 221, 154-169.

A

Appendix 1

Table A.1: General, Mechanical, Groundwater, Thermal, Initial

Parameter	Linear elastic model
γ_{unsat} (N/m^3)	$18 * 10^3$
γ_{sat} (N/m^3)	$18 * 10^3$
e_{init} (-)	0.3
K_x (m/s)	use default
K_y (m/s)	use default
c_s $(J/kg/K)$	2000
λ_s $(W/m/K)$	4
E_{ref} (N/m^2)	$40 * 10^6$
ν	0.4
ρ_s (t/m^3)	2.6

Table A.2: Model parameters: Water and ice

Parameter	Value
T_{ref} (K)	274.16
γ_{water} (kN/m^3)	10
c_{water} $(J/t/K)$	$4.181 * 10^6$
λ_{water} $(W/m/K)$	0.6
L_{water} (J/t)	$334 * 10^6$
α_{water} $(1/K)$	$0.21 * 10^{-3}$
T_{water} (K)	274.16
c_{ice} $(J/t/K)$	$2.108 * 10^6$
λ_{ice} $(W/m/K)$	2.22
α_{ice}	$0.050 * 10^{-3}$

Table A.3: Soil properties: General, Groundwater, Thermal and Initial

Parameter	Value
General	
γ_{unsat} (kN/m^3)	18
γ_{unsat} (kN/m^3)	18
e_0 (-)	1.5
Groundwater	
K_x (m/s)	$1 * 10^{-5}$
K_y (m/s)	$1 * 10^{-5}$
Thermal	
C_s $(J/kg/K)$	2000
λ_{s1} $(W/m/K)$	1.5
ρ_s (kg/m^3)	2200
α_x $(1/K)$	$5 * 10^{-6}$
α_y $(1/K)$	$5 * 10^{-6}$
α_z $(1/K)$	$5 * 10^{-6}$
Initial	
$K_{0.x}$ (-)	0.5
$K_{0,y}$ (-)	0.5

Table A.4: Froze/unfrozen material properties for freezing-thawing cycle

Parameter	Value
Model-ID	15211522
T_{ref} (K)	273.16
$E_{f,ref}$ (kN/m^2)	$500 * 10^3$
$E_{f,inc}$ $(kN/m^2/K)$	10000
ν_f $(-)$	0.31
G_0 (kN/m^2)	10430
κ_0 $(-)$	0.03
p_c^* (kN/m^2)	-100
λ_0 $(-)$	0.1
γ $(-)$	1
k_t $(-)$	0.07
M $(-)$	1.2
λ_s $(-)$	0.6
κ_s $(-)$	$0.2 * 10^{-3}$
r $(-)$	0.6
β (m^2/kN)	$8 * 10^{-3}$
λ_r $(-)$	0.2
ρ_r (kN/m^2)	$1 * 10^6$
α $(-)$	9
T_{0ref} (K)	273.16
p_{ref} (kN/m^2)	$-395 * 10^3$
m $(-)$	1
p_{y0}^* AT Y_{ref} $(kN/m^2/m)$	-300
Y_{ref} (m)	15
Δp_{y0}^* $(kN/m^2/m)$	-20
e_0 $(-)$	1.5
$(S_{seg})_{in}$ (kN/m^2)	3500
p_{at} (kN/m^2)	-100
K_w (kN/m^2)	10^6

B

Appendix 2

Time [day]	Δ Temperature [K]	Temperature [K]	Temperature [°C]
1	-14	259.15	-14
2	-13	260.15	-13
3	-12	261.15	-12
4	-11	262.15	-11
5	-10	263.15	-10
6	-9	264.15	-9
7	-8	265.15	-8
8	-7	266.15	-7
9	-6	267.15	-6
10	-5	268.15	-5
11	-4	269.15	-4
12	-3	270.15	-3
13	-2	271.15	-2
14	-1	272.15	-1
15	0	273.15	0
16	1	274.15	1

Table B.1: Temperature function: Climate conditions - Winter to spring

Time [day]	Δ Temperature [K]	Temperature [K]	Temperature [°C]
1	4	277.15	4
2	3	276.15	3
3	2	275.15	2
4	2.5	275.65	2.5
6	1	274.15	1
7	0	273.15	0
8	0	273.15	0
9	0	273.15	0
10	-1	272.15	-1
11	-2	271.15	-2
12	-3	270.15	-3
13	-5	268.15	-5
14	-7	266.15	-7
15	-10	263.15	-10

Table B.2: Temperature function: Climate conditions - Autumn to Winter

Time [day]	Δ Temperature [K]	Temperature [K]	Temperature [°C]
1	0	273.15	0
1.5	-1	272.15	-1
2	-2	271.15	-2
2.5	-3	270.15	-3
3	-4	269.15	-4
3.5	0	273.15	0
5	2	275.15	2
5.5	3	276.15	3
6	4	277.15	4
7	6	279.15	6
8	10	283.15	10
12	15	288.15	15
14	20	293.15	20

Table B.3: Temperature function: Thermal flow - thawing

Time [day]	Δ Temperature [K]	Temperature [K]	Temperature [°C]
1	2	275.15	2
2	1	274.15	1
2.5	0.5	273.65	0.5
4	0	273.15	0
5	0	273.15	0
6	-2	271.15	-2
8	-5	268.15	-5
10	-7	266.15	-7
12	-10	263.15	-10
14	-15	258.15	-15
16	-16	257.15	-16
20	-22	251.15	-22

Table B.4: Temperature function: Thermal flow - freezing

C

Appendix 3

Surface Transfer	Day	SF from hand calculations
Climate conditions: Thawing		
$1W/m^2/K$	20 days	7.42
$1W/m^2/K$	50 days	7.41
$1W/m^2/K$	100 days	7.42
$1W/m^2/K$	150 days	7.42
Climate conditions: Freezing		
$1W/m^2/K$	20 days	7.41
$1W/m^2/K$	50 days	7.38
$1W/m^2/K$	100 days	7.30
$1W/m^2/K$	150 days	7.24
Climate conditions: Thawing		
$5W/m^2/K$	20 days	7.38
$5W/m^2/K$	50 days	7.39
$5W/m^2/K$	100 days	7.42
$5W/m^2/K$	150 days	7.42
Climate conditions: Freezing		
$5W/m^2/K$	20 days	7.34
$5W/m^2/K$	50 days	7.25
$5W/m^2/K$	100 days	7.27
$5W/m^2/K$	150 days	7.25
Climate conditions: Thawing		
$10W/m^2/K$	20 days	7.38
$10W/m^2/K$	50 days	7.41
$10W/m^2/K$	100 days	7.44
$10W/m^2/K$	150 days	7.44
Climate conditions: Freezing		
$10W/m^2/K$	20 days	7.30
$10W/m^2/K$	50 days	7.26
$10W/m^2/K$	100 days	7.25
$10W/m^2/K$	150 days	7.24

Table C.1: SF calculations using hand calculations - Climate conditions

Surface Transfer	Day	SF from python	Xc	Yc	R
Climate conditions: Thawing					
$1W/m^2/K$	20 days	7.20	20.40	21.20	13
$1W/m^2/K$	50 days	7.20	20.40	21.20	13
$1W/m^2/K$	100 days	7.20	20.40	21.20	13
$1W/m^2/K$	150 days	7.20	20.40	21.20	13
Climate conditions: Freezing					
$1W/m^2/K$	20 days	7.18	20.40	21.20	13
$1W/m^2/K$	50 days	7.18	20.40	21.20	13
$1W/m^2/K$	100 days	7.18	20.40	21.20	13
$1W/m^2/K$	150 days	7.18	20.40	21.20	13
Climate conditions: Thawing					
$5W/m^2/K$	20 days	7.08	20.40	21.20	13
$5W/m^2/K$	50 days	7.08	20.40	21.20	13
$5W/m^2/K$	100 days	7.08	20.40	21.20	13
$5W/m^2/K$	150 days	7.08	20.40	21.20	13
Climate conditions: Freezing					
$5W/m^2/K$	20 days	7.01	20.40	21.20	13
$5W/m^2/K$	50 days	7.01	20.40	21.20	13
$5W/m^2/K$	100 days	7.01	20.40	21.20	13
$5W/m^2/K$	150 days	7.01	20.40	21.20	13
Climate conditions: Thawing					
$10W/m^2/K$	20 days	7.07	20.40	21.20	13
$10W/m^2/K$	50 days	7.07	20.40	21.20	13
$10W/m^2/K$	100 days	7.07	20.40	21.20	13
$10W/m^2/K$	150 days	7.07	20.40	21.20	13
Climate conditions: Freezing					
$10W/m^2/K$	20 days	6.92	20.40	21.20	13
$10W/m^2/K$	50 days	6.92	20.40	21.20	13
$10W/m^2/K$	100 days	6.92	20.40	21.20	13
$10W/m^2/K$	150 days	6.92	20.40	21.20	13

Table C.2: SF calculations using python - Climate conditions

Day	SF from hand calculations
Thermal flow: Thawing	
20 days	5.30
50 days	5.30
100 days	5.31
150 days	5.32
Thermal flow: Freezing	
20 days	4.85
50 days	4.91
100 days	4.90
150 days	4.87

Table C.3: SF calculations hand calculations - Thermal flow

Day	SF from hand calculations	Xc	Yc	R
Thermal flow: Thawing				
20 days	5.30	20.40	21.20	13
50 days	5.30	20.40	21.20	13
100 days	5.31	20.40	21.20	13
150 days	5.32	20.40	21.20	13
Thermal flow: Freezing				
20 days	4.85	20.40	21.20	13
50 days	4.91	20.40	21.20	13
100 days	4.90	20.40	21.20	13
150 days	4.87	20.40	21.20	13

Table C.4: SF calculations using python - Thermal flow

DEPARTMENT OF ARCHITECTURE AND CIVIL ENGINEERING
CHALMERS UNIVERSITY OF TECHNOLOGY
Gothenburg, Sweden
www.chalmers.se

CHALMERS
UNIVERSITY OF TECHNOLOGY